NASA/TM-2021-104606/Vol. 57

Technical Report Series on Global Modeling and Data Assimilation, Volume 57

Randal D. Koster, Editor

Tendency Bias Correction in the GEOS AGCM

Yehui Chang, Siegfried Schubert, Randal Koster and Andrea Molod

August 2021

NASA STI Program ... in Profile

Since its founding, NASA has been dedicated to the advancement of aeronautics and space science. The NASA scientific and technical information (STI) program plays a key part in helping NASA maintain this important role.

The NASA STI program operates under the auspices of the Agency Chief Information Officer. It collects, organizes, provides for archiving, and disseminates NASA's STI. The NASA STI program provides access to the NTRS Registered and its public interface, the NASA Technical Reports Server, thus providing one of the largest collections of aeronautical and space science STI in the world. Results are published in both non-NASA channels and by NASA in the NASA STI Report Series, which includes the following report types:

- TECHNICAL PUBLICATION. Reports of completed research or a major significant phase of research that present the results of NASA Programs and include extensive data or theoretical analysis. Includes compilations of significant scientific and technical data and information deemed to be of continuing reference value. NASA counterpart of peer-reviewed formal professional papers but has less stringent limitations on manuscript length and extent of graphic presentations.

- TECHNICAL MEMORANDUM. Scientific and technical findings that are preliminary or of specialized interest, e.g., quick release reports, working papers, and bibliographies that contain minimal annotation. Does not contain extensive analysis.

- CONTRACTOR REPORT. Scientific and technical findings by NASA-sponsored contractors and grantees.

- CONFERENCE PUBLICATION. Collected papers from scientific and technical conferences, symposia, seminars, or other meetings sponsored or co-sponsored by NASA.

- SPECIAL PUBLICATION. Scientific, technical, or historical information from NASA programs, projects, and missions, often concerned with subjects having substantial public interest.

- TECHNICAL TRANSLATION. English-language translations of foreign scientific and technical material pertinent to NASA's mission.

Specialized services also include organizing and publishing research results, distributing specialized research announcements and feeds, providing information desk and personal search support, and enabling data exchange services.

For more information about the NASA STI program, see the following:

- Access the NASA STI program home page at http://www.sti.nasa.gov

- E-mail your question to help@sti.nasa.gov

- Phone the NASA STI Information Desk at 757-864-9658

- Write to:
  NASA STI Information Desk
  Mail Stop 148
  NASA Langley Research Center
  Hampton, VA 23681-2199

NASA/TM-2021-104606/Vol. 57

Technical Report Series on Global Modeling and Data Assimilation, Volume 57

Randal D. Koster, Editor

Tendency Bias Correction in the GEOS AGCM

Yehui Chang
Morgan State University, Baltimore, MD

Siegfried Schubert
Science Systems and Applications Inc., Lanham, MD

Randal Koster
Global Modeling and Assimilation Office (GMAO), NASA Goddard Space Flight Center, Greenbelt, MD

Andrea Molod
Global Modeling and Assimilation Office (GMAO), NASA Goddard Space Flight Center, Greenbelt, MD

National Aeronautics and
Space Administration

Goddard Space Flight Center
Greenbelt, Maryland 20771

August 2021

Level of Review: This material has been technically reviewed by technical management.

Available from

NASA STI Program
Mail Stop 148
NASA's Langley Research
Center Hampton, VA
23681-2199

National Technical Information
Service 5285 Port Royal Road
Springfield, VA 22161
703-605-6000

Table of Contents

List of Tables and Figures

Table 4. The bias correction for the M2_AGCM for *precipitation* in the NM region for TBC applied in the NM region (second column) and the contributions from the NM_2 (third column), NM_4 (fourth column), and NM_5 (fifth column), subregions, as well as the sum of the corrections from all 6 NM subregions (last column). The results show the decomposition of the inner product (in black, as a percent) in terms of an amplitude ratio (in blue, as a percent) and spatial similarity (in red) as defined by the RHS of equation 3 in the text. For the values to the left of the dashed lines, the biases are computed with respect to MERRA-2, and the values to the right of the dashed lines are the same except that the biases are computed with respect to ERA-5. See Fig. 2 for the definitions of the regions

Figure 1: A schematic of the model's climate drift. Here F is the forecast, O is the corresponding observational value, and the overbar denotes an average over a large number of forecasts. The example is for a positive model bias.

Figure 2: The 17 regions in which TBC was applied (see Table 1). The heavy black box outlines the NM region (a key focus of this study).

Figure 3: Results for the 250mb u-wind for each season. The left panels are the negative of the bias (MERRA-2 minus CNTRL) and the right panels are the impact of the TBC (TBC_GLOBAL minus CNTRL). Values are averaged over the period 1980-2017. Units are m/s.

Figure 4: Top panels: The contributions for each season to the global TBC impacts on the 250mb u-wind in the NM region from TBC in each of the zonal band subregions (NP, NM, TR, SM, SP). The last bar in each plot is the sum of the contributions from each zonal band. Bottom panels: The contributions for each season to the NM TBC impacts in the NM region from each subregion of NM (NM_1, NM_2, NM_3, NM_4, NM_5, NM_6). The last bar in each plot is the sum of the contributions from each subregion of NM. The values are the normalized inner products (I) as defined in eq. 3 of the text. See Table 1 and Figure 2 for the definitions of the regions.

Figure 5: Results for T2m for each season. The left panels are negative of the bias (MERRA-2 - CNTRL) and the right panels are the impact of the TBC (TBC_GLOBAL minus CNTRL). Values are averaged over the period 1980-2017. Units are °C.

Figure 6: Top panels: The contributions for each season to the global TBC impacts on T2m in the NM region from TBC in each of the zonal band subregions (NP, NM, TR, SM, SP). The last bar in each plot is the sum of the contributions from each zonal band. Bottom panels: The contributions for each season to the NM TBC impacts in the NM region from each subregion of NM (NM_1, NM_2, NM_3, NM_4, NM_5, NM_6). The last bar in each plot is the sum of the contributions from each subregion of NM. The values are the normalized inner products as defined in eq. 3 of the text. See Figure 2 for the definitions of the regions.

Figure 7: Results for precipitation for each season. The left panels are the negative of the bias (MERRA-2 - CNTRL) and the right panels are the impact of the TBC (TBC_GLOBAL minus CNTRL). Values are averaged over the period 1980-2017. Units are mm/day.

Figure 8: Top panels: The contributions for each season to the global TBC impacts on precipitation in the NM region from TBC in each of the zonal band subregions (NP, NM, TR, SM, SP). The last bar in each plot is the sum of the contributions from each zonal band. Bottom panels: The contributions to the NM TBC impacts in the NM region from each subregion of NM (NM_1, NM_2, NM_3, NM_4, NM_5, NM_6). The last bar in each plot is the sum of the contributions from each subregion of NM. The values are the normalized inner products as defined in eq. 3 of the text. See Figure 2 for the definitions of the regions.

Figure 9: T2m bias correction in NM_5 from TBC in various NM Subregions. The contributions from the NM region and from the NM_2, NM_4, and NM_5 subregions, as well as the sum of the corrections from all 6 NM subregions, are shown. The biases are computed with respect to station observations (dark bars) or ERA-5 (light bars). The values are the normalized inner products as defined in eq. 3 of the text. See Figure 2 for the definitions of the regions.

Figure 10: Schematic of how the TBCs might be acting to influence the tendencies. This could be indirectly through the impacts on the physics and dynamics terms (solid arrows), or directly (dashed arrow).

Figure 11: Impacts for JJA of global TBC on a) total cloudiness (fraction of area), b) latent heat flux, c) sensible heat flux, d) longwave flux at the surface and, e) shortwave flux at the surface. In each

set of two panels the left panel is the negative of the bias (MERRA-2 minus CNTRL), and the right panel is TBC minus CNTRL. Values are averaged over the period 1980-2017. Units are: W/m^2.

Figure 12: Impacts for SON of global TBC on a) total cloudiness (fraction of area), b) latent heat flux, c) sensible heat flux, d) longwave flux at the surface and, e) shortwave flux at the surface. In each set of two panels the left panel is the negative of the bias (MERRA-2 minus CNTRL), and the right panel is TBC minus CNTRL. Values are averaged over the period 1980-2017. Units are: W/m^2.

Figure 13: Impacts for DJF of global TBC on a) total cloudiness (fraction of area), b) latent heat flux, c) sensible heat flux, d) longwave flux at the surface and, e) shortwave flux at the surface. In each set of two panels the left panel is the negative of the bias (MERRA-2 minus CNTRL), and the right panel is TBC minus CNTRL. Values are averaged over the period 1980-2017. Units are: W/m^2.

Figure 14: Impacts for MAM of global TBC on a) total cloudiness (fraction of area), b) latent heat flux, c) sensible heat flux, d) longwave flux at the surface and, e) shortwave flux at the surface. In each set of two panels the left panel is the negative of the bias (MERRA-2 minus CNTRL), and the right panel is TBC minus CNTRL. Values are averaged over the period 1980-2017. Units are: W/m^2.

Figure 15: Impact of TBC on the 250mb eddy (deviations from the zonal mean) height field compared to the model bias. The left panels are the negative of the bias with respect to MERRA-2. The right panels show the impact of TBC. The top panels are for the M2_AGCM (averaged for the period 1980-2017). The bottom panels are for the updated model (the IC_AGCM), averaged for the period 1981-2016. Units are meters. The box in each figure outlines our region of interest - the Pacific/North American region.

Figure 16: A schematic of the replay approach used to compute the analysis increments (IAU, or Δx in our current terminology) from an existing analysis (figure taken from Chang et al. 2019). Here IAU refers to the incremental analysis update procedure for performing data assimilation developed by Bloom et al. (1996). See also Takacs et al. 2018 for further information about the numerical stability of replay.

Figure 17: The impact of global and regional TBC on the 250mb height field for the IC_AGCM. a) negative of the bias with respect to MERRA-2, b) the impact of global TBC, c) the sum of the impacts from the tropical (TR) and northern middle latitude (NM) TBC, d) impact of TR TBC, e) impact of

NM TBC, f) impact of applying TBC in the region that combines TR_2 and TR_3 and TR_4. Results are averages for the period 1981-2016. Units are meters.

Figure 18: Same as Fig. 17, except for the precipitation. Units are mm/day.

Figure 19: Long term averages (1980-2016, denoted by an overbar) of the various terms of the JJA mean temperature (T) tendency at 850mb computed from MERRA-2. The top 6 panels show the contributions to the tendency from the various physical terms in the thermodynamic equation such that $\frac{\partial \bar{T}}{\partial t} = \overline{dynamics} + \overline{moist} + \cdots + \overline{\triangle T} \cong 0$, where $\overline{\triangle T}$ (lower middle panel) is the long-term average analysis increment of temperature. The lower left panel is the sum (total) of all the physical terms. The lower right panel shows that the long-term average of the sum of the physical terms and the analysis increment is indeed effectively zero. Units: °C/day.

Figure 20: Long term averages (1980-2016, denoted by an overbar) of the various terms of the JJA mean specific humidity (q) tendency at 850mb computed from MERRA-2. The top panels show the contributions to the tendency from the various physical terms in the moisture equation. Here, $\frac{\partial \bar{q}}{\partial t} = \overline{dynamics} + \overline{moist} + \cdots + \overline{\triangle q} \cong 0$, where $\overline{\triangle q}$ (lower middle panel) is the long-term average analysis increment of specific humidity. The lower left panel is the sum (total) of all the physical terms. The lower right panel shows that the long-term average of the sum of the physical terms and the analysis increment is indeed effectively zero. Units are g/day.

Figure 21: An example of the αs for surface pressure for January and July.

Figure 22: A comparison of the results for TBC and TBC together with a state-dependent term (SD_TBC) for JJA for the 850mb u-wind (m/s, left panels) and the 250mb v-wind variance ($(m/s)^2$, right panels).

Executive Summary

The Global Modeling and Assimilation Office (GMAO) recently developed an approach for correcting long-term biases in climate models. The approach, called tendency bias correction (TBC), introduces additional forcing terms into the model's prognostic equations based on the long-term (multi-decade) averages of short term (typically 6 hour) forecast errors. The approach was further generalized to allow limiting the TBC to specific regions of the globe, thereby providing insights into those regions of the global where model errors have the largest impact on climate bias.

In this report, we summarize the results of global and regional TBC applied to the GEOS AGCM (the same model used to generate MERRA-2 though run at lower resolution, referred to as the M2_AGCM) employing the analysis increments (analysis minus forecast) generated by MERRA-2 to calculate the TBC terms. Extending the results of Chang et al. (2019) and Schubert et al. (2019), we examine in more detail the seasonality of the TBC impacts, including a deeper look into the reasons for why TBC appears to be least effective during boreal winter. We also look into the ability of TBC to correct other diagnostic fields such as cloudiness and surface fluxes and, more generally, attempt to provide some insight into why TBC is effective in correcting long term climate biases. Looking beyond TBC, we also present some preliminary results from an extension of the TBC approach in which we include a state-dependent term.

Focusing on the Northern Hemisphere (NH) middle latitude impacts, the results show a substantial seasonality in the efficacy of TBC in correcting many of the long-standing circulation biases (e.g., upper-level jets and stationary waves) of the M2_AGCM, with the summer season showing the greatest improvements and the winter season showing the least. A key difference between JJA and

DJF is the fact that the contributions to the TBC impacts in the Northern Hemisphere middle latitudes tend to be local in summer. That is, the sources of the TBC impacts in middle latitudes are largely confined to the middle latitudes, while during the winter there are substantial contributions to the impacts in the middle latitudes from other latitude bands, especially from the tropics. The transition season impacts are somewhere in between, with SON behaving more like JJA, and MAM behaving more like DJF. During all seasons (though less so for DJF) we see an important impact on the climate bias in the NH middle latitudes coming from TBC in a region encompassing the Tibetan Plateau, highlighting the importance of correcting the model biases in that very mountainous region. Similarly, we found a substantial seasonality in the ability of TBC to correct the climate biases in the surface meteorology over North America, with TBC correcting about 60% of the bias in T2m and more than 50% of the bias in precipitation during JJA. In contrast, during DJF, TBC corrects only about 30% of the bias in T2m and less than 20% of the bias in precipitation.

The impacts on other diagnostic fields (total cloudiness, latent and sensible heat fluxes and the long-wave and short-wave radiation fluxes) also show substantial improvements, but that improvement has a strong seasonality with the largest improvements again occurring in JJA and the smallest improvements occurring in DJF. While we cannot rule out the possibility that the TBCs are introducing some artificial corrections that circumvent the model physics, the improvements in the cloudiness and surface fluxes indicate that the improvements in the climate biases from TBC is, at least in part, the result of improved input (the prognostic quantities) to the relevant parameterizations, leading to physically realistic improvements (via the physical parametrizations) to such fields as T2m and precipitation.

The reasons for the smaller impacts in the NH during DJF are still somewhat unclear, though a distinguishing feature of that season is the greater importance of tropical heating errors in contributing to NH middle latitude stationary wave biases. Using an updated GEOS AGCM (though with boreal winter stationary wave biases that are very similar to those of the M2_AGCM) we found that the TBCs obtained from employing a technique called "*replay*" developed in the GMAO to generate the short-term forecast errors did produce improved stationary waves and related fields, and those improvements appear to be the result of improved tropical heating with TBC. This apparent sensitivity of the results to how the TBCs are produced (in the case of the M2_AGCM they were simply taken from the MERRA2 archive) is of some concern, but highlights the need to compute the short-term forecast errors (and the TBCs) for the model in question directly, in either a data assimilation or replay environment.

We also look more generally at the reasons why TBC seems to work, looking in particular at the size of the TBCs relative to the physical and dynamical forcing terms in the model. The results show that the TBCs overall tend to be relatively small, suggesting the model's response to the TBCs is likely linear, though that is less true for the moisture in the tropics where the TBCs can have amplitudes locally that rival those of the physical terms. We in fact do find considerable double counting (nonlinearity) when examining the separate impacts of TBC from different regions, and this appears to be especially true for precipitation, and for DJF during which the impacts from the tropics is important.

Finally, we present some initial results of an extension to TBC that includes a state-dependent term. The motivation for such an extension is that by minimizing the error in the time tendency, such a term could potentially produce a greater positive impact (compared with the original TBC approach)

on forecast skill. The results we have obtained so far highlight some of the challenges one faces in producing statistically robust estimates of state-dependent terms, and in introducing them in a way that maintains model stability.

1.0 Review of TBC and focus of this report

Recently Chang et al (2019) introduced the tendency bias correction (TBC) approach for correcting biases in climate models. The TBC approach, described in more detail below, uses information about biases in short-term (e.g., 6 hour) forecast errors to calculate constant correction terms that are introduced into the model's prognostic equations. Schubert et al. (2019) extended the approach to allow limiting the TBC to specific regions (termed "regional TBC"), thereby providing a systematic approach to identifying how model errors in any one region impact climate bias across the globe.

In this report we expand on the results of Chang et al (2019) and Schubert et al (2019) by delving further into the ability of TBC (both global and regional) to correct the climate biases of the GEOS AGCM, looking in more detail at the impacts during all seasons, as well as the impacts on additional diagnostic fields (e.g., surface fluxes and cloudiness) that provide further insights into how TBC acts to correct long term climate biases. We also look further into the reasons for the relatively poor performance of the TBC in the boreal winter hemisphere. More generally, we discuss both why TBC seems to work, and what may be fundamental limitations to TBC, especially regarding the interpretation of regional TBC results. Finally, we introduce an extension of the TBC methodology to include a state-dependent term.

Our approach to TBC takes advantage of the incremental analysis update (IAU) procedure (Bloom et al. 1996) employed in the GEOS data assimilation system (Rienecker et al. 2008) in which the equations governing the assimilation have the form:

$$\frac{\partial x}{\partial t} = f(x) + \Delta x \qquad (1),$$

where $\Delta x = (analysis - forecast)/6hrs$ is the instantaneous analysis increment (applied to the model's prognostic variables: temperature, winds, humidity, surface pressure and ozone), and f(x) consists of all the dynamics and physics terms of the model (basically the uncorrected model). Following Chang et al. (2019), the governing equations for the TBC approach have the same form as (1), except that now the forcing term is a long term mean of the increments. In particular,

$$\frac{\partial x}{\partial t} = f(x) + \overline{\Delta x} \qquad (2),$$

where $\overline{\Delta x}$ is the time average (denoted by the overbar) of the instantaneous Δx values computed here over the years 1980 - 2017. In the above, $\overline{\Delta x}$ is the tendency bias correction (TBC) term. The averaging is done independently for different times of the day and for different times of the year; in this way, we retain the diurnal and annual cycles in the TBCs. It is important to emphasize that the TBC approach only makes use of information about the initial short-term forecast errors and furthermore only the long-term average of those (tendency) errors. As such, it is not at all clear that correcting tendency biases should have a substantial impact on the model's long-term climate biases (Figure 1). In fact, as we shall see, TBC does correct long term climate biases, and we attempt to address why that is the case later in this report. It is also worth noting that TBC appears to provide only modest improvements to forecast skill (Chang et al. 2019) – something we address in this report in terms of a potential extension of TBC that more directly addresses tendency errors.

In the following, we will look in detail at the impacts of TBC (applied both globally and regionally) on the GEOS AGCM's long term climate biases. Section 2 describes the verification data sets, the GEOS AGCM, and the various model experiments. The results are presented in Section 3. In Section 4 we discuss the advantages and limitations of TBC as well as a possible extension to TBC involving a state-dependent correction term. The summary and conclusions are given in Section 5.

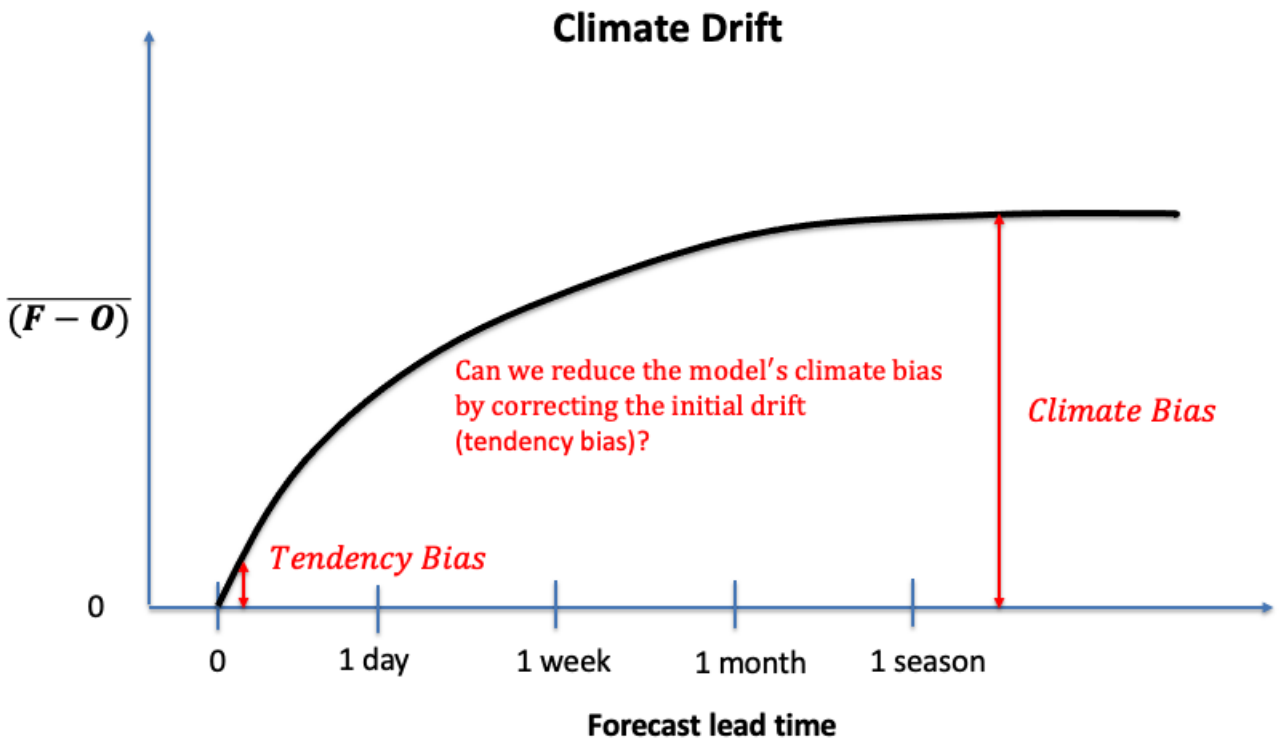

Figure 1: A schematic of the model's climate drift. Here F is the forecast, O is the corresponding observational value, and the overbar denotes an average over a large number of forecasts. The example is for a positive model bias.

2. Experiments and Datasets

2.1 MERRA-2 and other observational datasets

The atmospheric reanalysis data used for this study is the Modern-Era Retrospective analysis for Research and Applications version 2 (MERRA-2; Gelaro et al. 2017). MERRA-2, developed by NASA Goddard Space Flight Center (GSFC) / Global Modeling and Assimilation Office (GMAO), is an updated version of MERRA (Rienecker et al. 2011) including an improvement of the assimilating model's physical parameterizations of moist processes, turbulence, land and ocean surface processes, and gravity wave drag (Bosilovich et al. 2015; Molod et al. 2015; Gelaro et al. 2017; see also below). Other differences from MERRA include aerosol data assimilation, as well as new developments in the representation of ozone and the use of precipitation observations to force the land surface. The horizontal resolution of the MERRA-2 data is 0.625° longitude × 0.5° latitude. The key variables used here consist of 2-meter air temperature (T2M), precipitation (the raw values from model, i.e., the values not yet corrected by observations), zonal wind, and geopotential height. We note that the MERRA-2 precipitation used in this study for verification is an observationally-corrected product in which the precipitation generated by the atmospheric model underlying MERRA-2 was merged with gauge and satellite precipitation observations (Reichle and Liu 2014, Reichle et al. 2017). In the following, we will use the words observations and MERRA-2 interchangeably with, of course, the understanding that MERRA-2 is a reanalysis product that combines a model-based first guess with observations and, as such, the reanalysis products are potentially impacted by model biases.

While most of our validation of the TBC results is done against MERRA-2, we also, on a more limited basis, validate against ERA-5 (C3S 2017), and two station-based observational datasets: the gridded GHCN_CAMS data for T2m over land (Fan and van den Dool 2008), and the GPCP V2.3 for precipitation (Adler et al. 2003).

2.2 The GEOS AGCM

Most of the results presented here are based on the same version of the GEOS AGCM that was used to generate MERRA-2, though run here at a lower horizontal resolution (approximately 1°); we refer to this as the M2_AGCM. As described in Gelaro et al. (2017), M2_ AGCM includes the finite-volume dynamical core of Putman and Lin (2007), which uses a cubed sphere horizontal discretization at an approximate resolution of 0.5° × 0.625°, with 72 hybrid-eta levels from the surface to 0.01 hPa. Recent upgrades to the physical parameterization schemes include increased re-evaporation of frozen precipitation and cloud condensate, changes to the background gravity wave drag, and an improved relationship between the ocean surface roughness and ocean surface stress (Molod et al. 2015). The model also includes a Tokioka-type trigger on deep convection as part of the Relaxed Arakawa-Schubert (RAS, Moorthi and Suarez 1992) convective parameterization scheme, which governs the lower limit on the allowable entrainment plumes (Bacmeister and Stephens 2011). The implementation of new glaciated land representation and seasonally-varying sea ice albedo produced improved air temperatures and reduced biases in the net energy flux over these surfaces (Cullather et al. 2014). The model includes the Catchment land surface model developed by Koster et al. (2000). Further details about the GEOS AGCM can be found in Molod et al. (2015).

While most of the results presented here are based on the M2_AGCM described above, a few results (presented in Section 3.3) are based on a newer version of the GEOS AGCM. This interim development version of the model (Icarus-3_3_p2, referred to hereafter as the IC_AGCM) was also run at 1° horizontal resolution.

2.3 The TBC Simulations

As mentioned above, all of the simulations described here (with the exception of the results shown in Section 3.3) were produced with the same version of the GEOS AGCM that was used to produce MERRA-2 (the M2_AGCM). The runs were made with the same SST data, greenhouse gases (GHGs), and other forcing used to produce MERRA-2. The only differences are that the M2_AGCM was run at coarser resolution and, of course, that the simulations did not assimilate observations. This similarity offers the unique opportunity to assess how the observations influence various aspects of the model climate, but of course to the extent that any model errors are reflected in the reanalysis, it also has the potential to bias our assessment of model errors. We address the latter in a limited way, by computing the model's climate biases using several different verification datasets.

The main set of experiments with the M2_AGCM examined here are identical to those described in Schubert et al. (2019) and are, for convenience, listed in Table 1. All the runs are forced with observed SST and span the period 1980-2017. These include a control run without TBC applied (CNTL), a run in which the TBC is applied globally (TBC_GLOBAL), and 17 runs in which the TBC is applied over specified regions (see Figure 2). The 17 regions consist of 5 zonal bands (the Northern Polar region or NP, the Northern Middle latitudes or NM, the Tropical Region or TR, the Southern

Middle latitudes or SM, and the Southern Polar region or SP). The NM and TR latitudinal bands are each split into six sub-regions. As mentioned above, the runs listed in Table 1 were repeated with an updated version of the GEOS-AGCM (IC_AGCM) for a slightly shorter time period (1981-2016). In addition, we carried out an experiment with the IC-AGCM in which TBC was applied to a larger tropical subregion spanning much of the Indian and Pacific Oceans (combining regions TR_2, TR_3 and TR_4) as described in Section 3.3.

Table 1. A summary of the GEOS AGCM experiments. See Fig. 2 for definitions of the regions. The AGCM is the MERRA-2 version of the model (M2_AGCM). For some of the results shown in Section 3.3, however, the experiments were repeated using a more recent version of the model (IC_AGCM) for the period 1981-2016 (see text for details).

Exp. #	Exp. Name	Description	Model
1	CNTL	37- year control simulation for the period 1980-2017	Uncorrected AGCM
2	TBC_NP TBC_NM TBC_TR TBC_SM TBC_SP	37- year simulations for the period 1980-2017 in which TBC is applied to selected zonal bands	AGCM with TBC
3	TBC_NM1 TBC_NM2 TBC_NM3 TBC_NM4 TBC_NM5 TBC_NM6	37- year simulations for the period 1980-2017 in which TBC applied to selected regions spanning the NM region	AGCM with TBC
4	TBC_TR1 TBC_TR2 TBC_TR3 TBC_TR4 TBC_TR5 TBC_TR6	37- year simulations for the period 1980-2017 in which TBC is applied to selected regions spanning the TR region	AGCM with TBC
5	TBC_GLOBAL	37- year simulations for the period 1980-2017 in which TBC is applied globally	AGCM with TBC

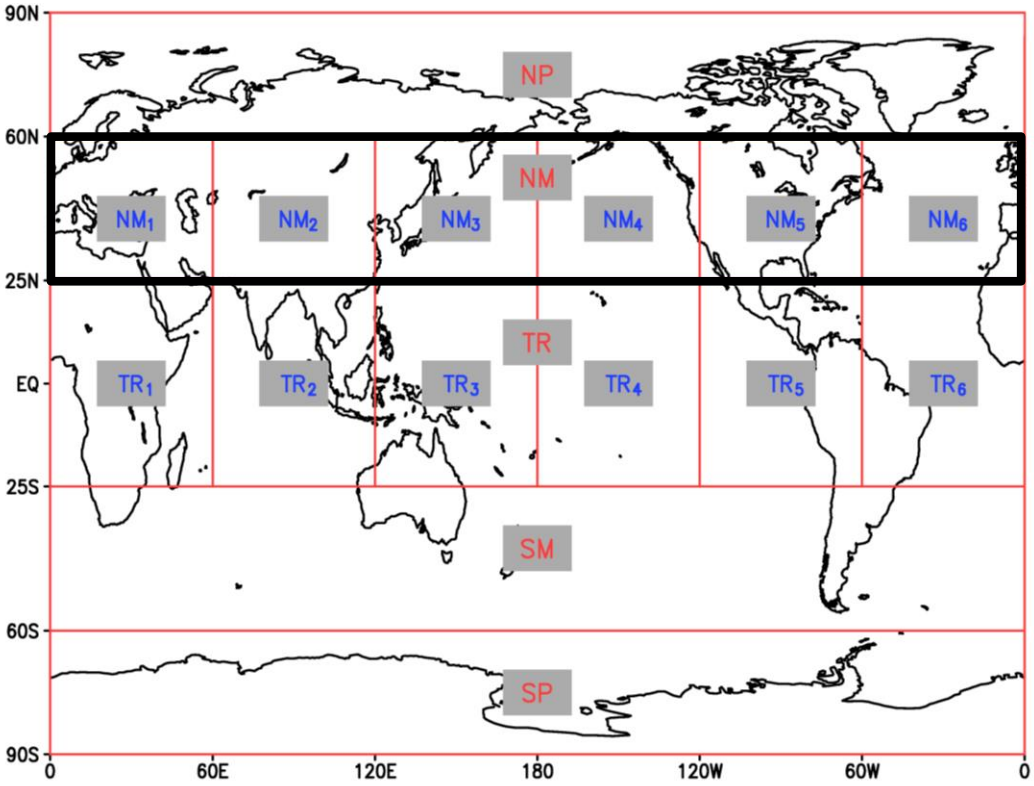

Figure 2: The 17 regions in which TBC was applied (see Table 1). The heavy black box outlines the NM region (a key focus of this study).

3. Results of TBC

In assessing the efficacy of the TBC approach, we distinguish in the following between "impact" and "bias correction", with the former being an assessment of how TBC influences the model's climate, and the latter being an assessment of the extent to which TBC actually corrects the model's climate bias (i.e., to what extent do the impacts of TBC project onto the climate bias). These are quantified with an inner product measure (Schubert et al. 2019):

$$\mathrm{I} = \frac{X \bullet Y}{|Y|^2} = \frac{|X|}{|Y|} cos\theta \,, \qquad (3)$$

where X and Y are vectors with components x_j and y_j, respectively, at the grid points (j) making up a particular region. Here X and Y can refer to the results (TBC minus control) of two different TBC runs (when addressing impacts) or, in the case of assessing climate bias correction, Y refers to the climate bias (control minus observed)[1]. The former (addressing impacts) is especially important for quantifying the contributions made to the impact of TBC applied in one region (e.g., the NM region, see Figure 2), from TBC applied to various subregions (e.g., NM_1, NM_2 ..., etc.), thereby allowing us to potentially identify those subregions having the largest impacts. The right-hand side of (3) indicates that the inner product between X and Y can be written as the ratio of the magnitudes of the vectors, multiplied by the cosine of the angle (θ) between the two vectors (a measure of spatial similarity).

We shall see that regional TBC does not always produce results that are easy to interpret. Specifically, the results are in some cases (especially for precipitation) not linear in the sense that the sum of the responses (R_i, i=1,N) obtained when TBC is applied separately to each of the subregions making up a larger region add up to a value that is larger than the response (R) obtained when TBC is applied to that larger region. That is,

$$R_1 + R_2 + \ldots R_N > R \qquad (4).$$

[1] Here we actually compute (observed minus control) for the sign to be consistent with how we compute the impacts (TBC minus control).

This nonlinearity (which we refer to as double counting) appears to reflect the fact that improvements in one region appear to be coming from TBC applied to two (or more) different regions for which the tendency errors are not independent.

We begin in Section 3.1 by examining the extent to which global and regional TBC corrects the climates of the 250mb zonal wind, the 2-meter temperature (T2m) over land, and the precipitation. This includes an assessment of both how TBC applied to one region impacts the climate in other regions and the extent to which those impacts act to reduce the M2_AGCM's climate bias.

3.1 Efficacy of global and regional TBC in correcting key fields

a) u-wind at 250mb

Figure 3 shows the results of applying TBC globally for the 250mb u-wind for each season, with the bias (actually the negative of the bias with respect to MERRA-2) shown in the left panels and the TBC impacts (TBC minus CNTRL) shown in the right panels. Comparing the anomalies in the left and right panels, one finds a remarkable degree of similarity for all seasons. This is especially true for JJA (cf. Figs. 3e and f) where the large summer jet biases are substantially reduced. In fact, the percent of the 250mb u-wind bias corrected by global TBC (I, expressed as a percent) is 65%, 60%, 74%, and 58% for DJF, MAM, JJA and SON, respectively (see values in the right margin Fig. 3). The pattern similarity ($cos\theta$) is also substantial, with values ranging from 0.65 in SON to as high as 0.87 in JJA. The ratios of the magnitudes of the vectors (see 3) also show that TBC_GLOBAL corrects a substantial fraction of the bias with values ranging from a low of 0.79 for MAM to a high of 0.89 for SON. One result not reflected in the global inner products (but see the discussion of

Table 2 below), is the lack of a substantial correction to the DJF North Pacific jet bias (cf. Figs. 3a and b). We will look into the possible reasons for that in Section 3.3.

We next look in more detail at the nature of the TBC impacts on the 250mb zonal wind, focusing on the impacts in the NH middle latitudes (region NM, see Fig. 2). The top panels of Figure 4 show how much TBC, when applied separately to each of the different zonal bands, contributes to the impacts in the NM zonal band produced with global TBC. For each season it is clear that the TBC applied to the NM region is the main contributor to the impacts in that band. In the case of JJA (Fig. 4c), the TBC applied to the NM region accounts for essentially all the impact in that zonal band. Also, for both MAM and SON (Figs. 4b and d), TBC in the NM region accounts for more than 80% of the total impacts in the NM region. It is only for DJF (Fig. 4a) that other zonal bands contribute substantially to the NM impacts, with TBC from NP and TR together accounting for about 40% of the impact compared with 60% for the NM region. It is noteworthy that the SUM is greater than 1 (especially for SON, Fig. 4d), indicating that there is some double counting. We will come back to the double counting issue in our discussion of the limitations of regional TBC in Section 4.1.

Given the importance of TBC in the NM region, we next examine which subregions of NM seem to play an important role. To address that, we show in the bottom row of Figure 4 the contributions of the TBC applied to each of the six NM subregions to the total impact from TBC in the NM region. A key result is that the NM_2 region is an important contributor during all seasons, contributing between 40% and 60% of the total depending on the season. The reasons for the importance of the NM_2 region during JJA, as already discussed in Schubert et al. (2019), have to do with the substantial temperature biases of the M2_AGCM over and around the Tibet highlands. We now see that the

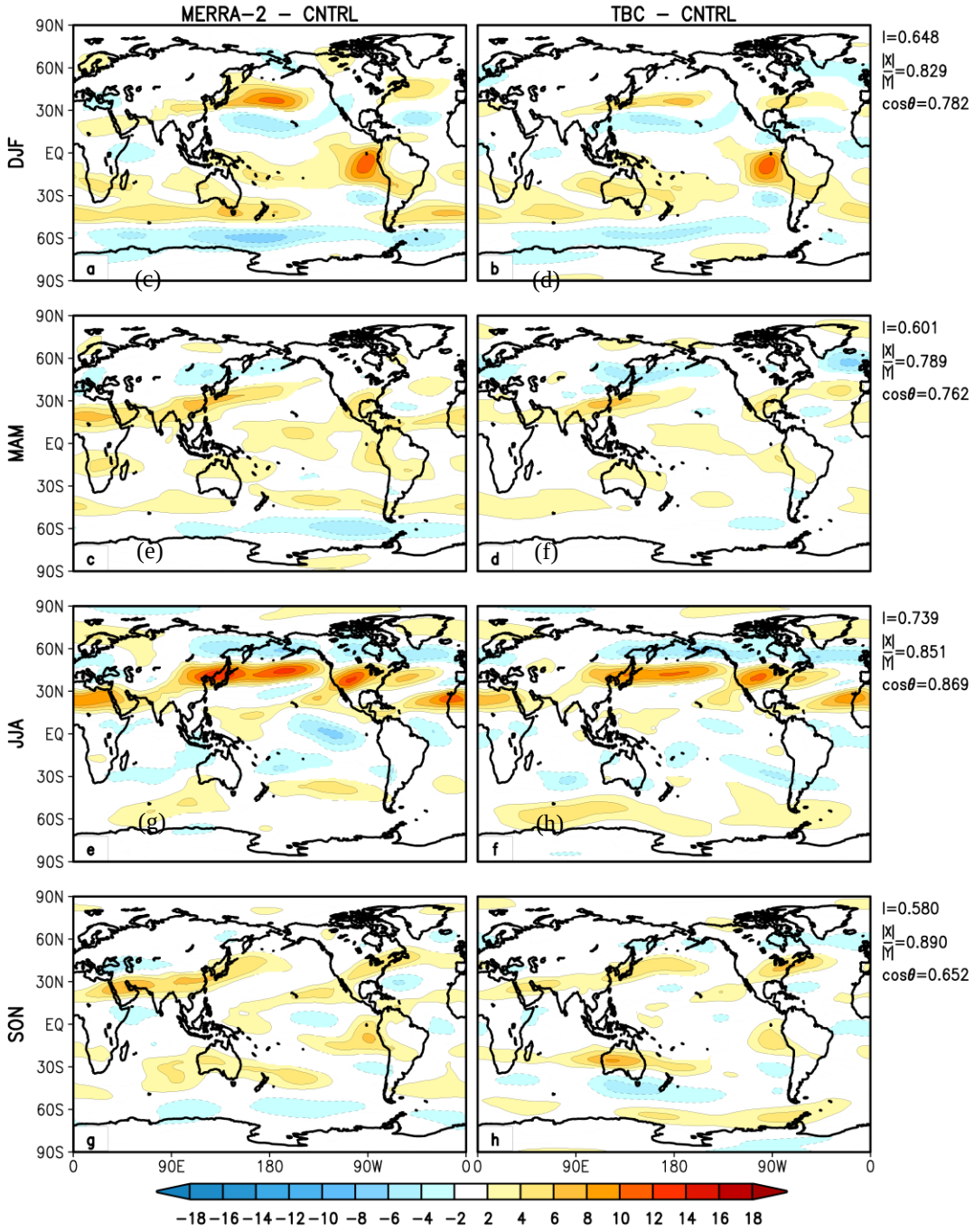

Figure 3: Results for the 250mb u-wind for each season. The left panels are the negative of the bias (MERRA-2 minus CNTRL) and the right panels are the impact of the TBC (TBC_GLOBAL minus CNTRL). Values are averaged over the period 1980-2017. Units are m/s.

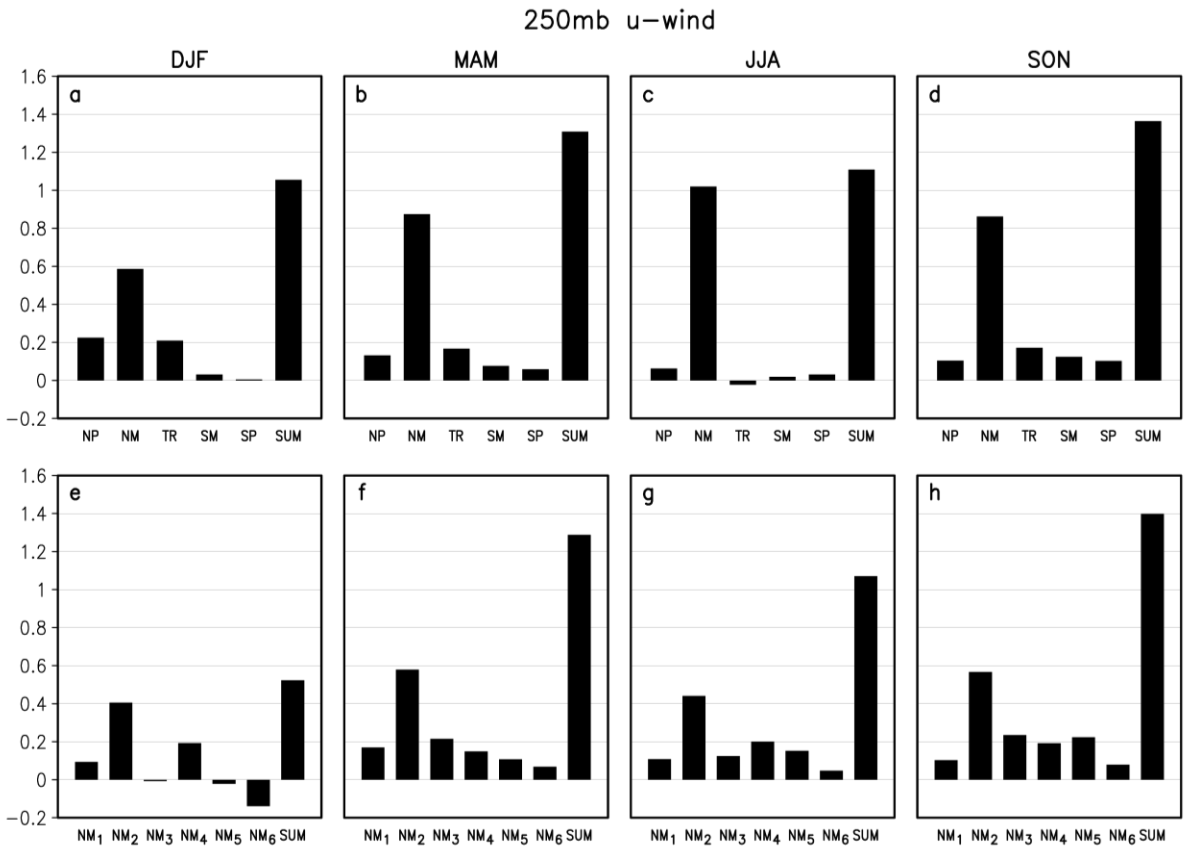

Figure 4: Top panels: The contributions for each season to the global TBC impacts on the 250mb u-wind in the NM region from TBC in each of the zonal band subregions (NP, NM, TR, SM, SP). The last bar in each plot is the sum of the contributions from each zonal band. Bottom panels: The contributions for each season to the NM TBC impacts in the NM region from each subregion of NM (NM_1, NM_2, NM_3, NM_4, NM_5, NM_6). The last bar in each plot is the sum of the contributions from each subregion of NM. The values are the normalized inner products (I) as defined in eq. 3 of the text. See Table 1 and Figure 2 for the definitions of the regions.

NM_2 region is also important for the other seasons; it is, in fact, even more important for both MAM (Fig. 4f) and SON (Fig. 4h), for which the NM_2 region accounts for nearly 60% of the total impact in the NM region, compared with about 40% for JJA.

Table 2 summarizes the u250mb u-wind climate bias corrections in the NM zonal band in terms of the inner product, the amplitude ratio and similarity (eq. 3). For each result, two numbers are shown (separated by dashed lines) corresponding to two different validation products used to compute the bias (MERRA-2 on the left and ERA-5 on the right). Overall, the results show that there is little difference between the two estimates of the bias for the 250mb u-wind. The percent of the u250mb wind bias in the NM region corrected by applying TBC to the NM region is shown in the second column of Table 2. The results show a strong seasonality to the bias correction in the NM region, with close to 90% corrected in JJA, about 70% during MAM and SON, and only about 20% during DJF. This is reflected in the spatial similarity which shows values of 0.91 for JJA, about 0.7 for MAM and SON, but only about 0.3 for DJF. The amplitudes of the corrections are reasonable (close to 100%) during all seasons except DJF, when the amplitude of the impact is only ¾ of the climate bias. The third, fourth and fifth columns of Table 2 show the contributions to the corrections in the NM region from TBC applied to regions NM_2, NM_4 and NM_5, respectively. These results are consistent with what we already saw for the impacts (Fig 4), with region NM_2 playing a key role. In particular, we see that TBC in NM_2 accounts for more than 50% of the bias correction in the NM region for MAM, about 45% for SON, 36% for JJA, but only about 20% for DJF. It is interesting that the spatial similarity from TBC in the NM_2 region is about 0.6 for all seasons except for DJF, when it is just over 0.4 (third column of Table 2). TBC applied to the other two regions (NM_4 and NM_5) account for considerably less of the bias correction in the NM region, though both JJA and SON do show values ranging from about 13% to 19%. It is noteworthy that both SON and MAM show considerable double counting, with the SUM (inner product of the sum of the corrections over all 6 subregions) for each exceeding 100%; the SUM is 115% and about 125% for SON and MAM, respectively, reflecting excessive amplitude ratios that exceed 200% in the case of MAM.

Table 2. The bias correction for the M2_AGCM for the 250mb u-wind in the NM region for TBC applied in the NM region (second column) and the contributions from the NM_2 (third column), NM_4 (fourth column), and NM_5 (fifth column) subregions, as well as the sum of the corrections from all 6 NM subregions (last column). The results show the decomposition of the inner product (in black, as a percent) in terms of an amplitude ratio (in blue, as a percent) and spatial similarity (in red) as defined by the RHS of equation 3 in the text. For the values to the left of the dashed lines, the biases are computed with respect to MERRA-2, and the values to the right of the dashed lines are the same except that the biases are computed with respect to ERA-5. See Fig. 2 for the definitions of the regions.

Season	bias corrected from TBC in NM region:		from TBC in NM_2		from TBC in NM_4		from TBC in NM_5		SUM	
JJA	**87.4**	**88.4**	**36.2**	**36.8**	**18.7**	**19.0**	**13.3**	**13.5**	**91.5**	**92.6**
	96.0	97.7	55.4	56.3	29.3	29.9	24.2	24.6	118.7	120.8
	0.91	0.91	0.65	0.65	0.64	0.64	0.55	0.55	0.77	0.77
SON	**68.0**	**67.7**	**45.1**	**44.9**	**16.5**	**16.6**	**17.8**	**17.6**	**115.0**	**115.4**
	98.4	99.0	75.1	75.6	39.1	39.4	42.1	42.3	193.3	194.5
	0.69	0.68	0.60	0.59	0.42	0.42	0.42	0.42	0.60	0.59
DJF	**21.0**	**22.2**	**19.9**	**20.3**	**9.0**	**8.7**	**-4.2**	**-4.5**	**26.3**	**25.8**
	74.9	74.4	46.1	45.8	50.2	49.9	39.5	39.2	157.7	156.6
	0.28	0.30	0.43	0.44	0.18	0.17	-0.11	-0.11	0.17	0.16
MAM	**72.9**	**73.1**	**52.0**	**53.1**	**11.6**	**11.9**	**11.1**	**11.3**	**122.7**	**126.3**
	104.9	106.6	81.6	82.8	52.2	53.0	50.2	51.0	228.9	232.3
	0.69	0.69	0.64	0.64	0.22	0.22	0.22	0.22	0.54	0.54

b) Temperature at 2 meters (T2m)

The results of TBC for T2m are shown in Fig. 5. Recall that the AGCM is forced with observed SSTs so we only show the results over land areas. The bias in T2m (left panels of Figure 5) has a strong seasonality, with DJF (Fig. 5a) having a substantial cold bias over northern Eurasia, Canada and parts of the U.S. (recall the figures show the negative of the bias), and JJA (Fig. 5e) displaying a strong warm bias in those same regions. The biases of the transition seasons fall in between the two extreme seasons, with MAM (Fig. 5c) displaying some of the cold bias of DJF, and SON (Fig. 5g) showing some of the warm bias of JJA. The global TBC acts to substantially correct the T2m biases (right panels of Fig. 5), though not to same extent that we saw previously for the 250mb u-wind. Here, the percent of the global T2m bias that is corrected is 40%, 51%, 60%, and 35%, for DJF, MAM, JJA and SON, respectively (see values in the right margin of Fig. 5). We note that the relatively low value of the inner product (I) in DJF (cf. Figs. 5a and b) is due to the weak amplitude (52%) of the correction rather than a low spatial similarity (it is relatively high at 0.77). In contrast, the relatively low value of the inner product (I) in SON (cf. Figs. 5g and h), is due to a rather low spatial similarity of the correction (0.45) rather than a weak amplitude (it has the relatively large value of 72%).

We next look in more detail at the nature of the T2m impacts, focusing again on the impacts in the NH middle latitude regions (region NM, see Fig. 2). The top panels of Figure 6 show how much TBC, when applied separately to each of the different zonal bands, contributes to the impacts seen in the NM zonal band from global TBC. The results are quite similar to what we saw for the 250mb

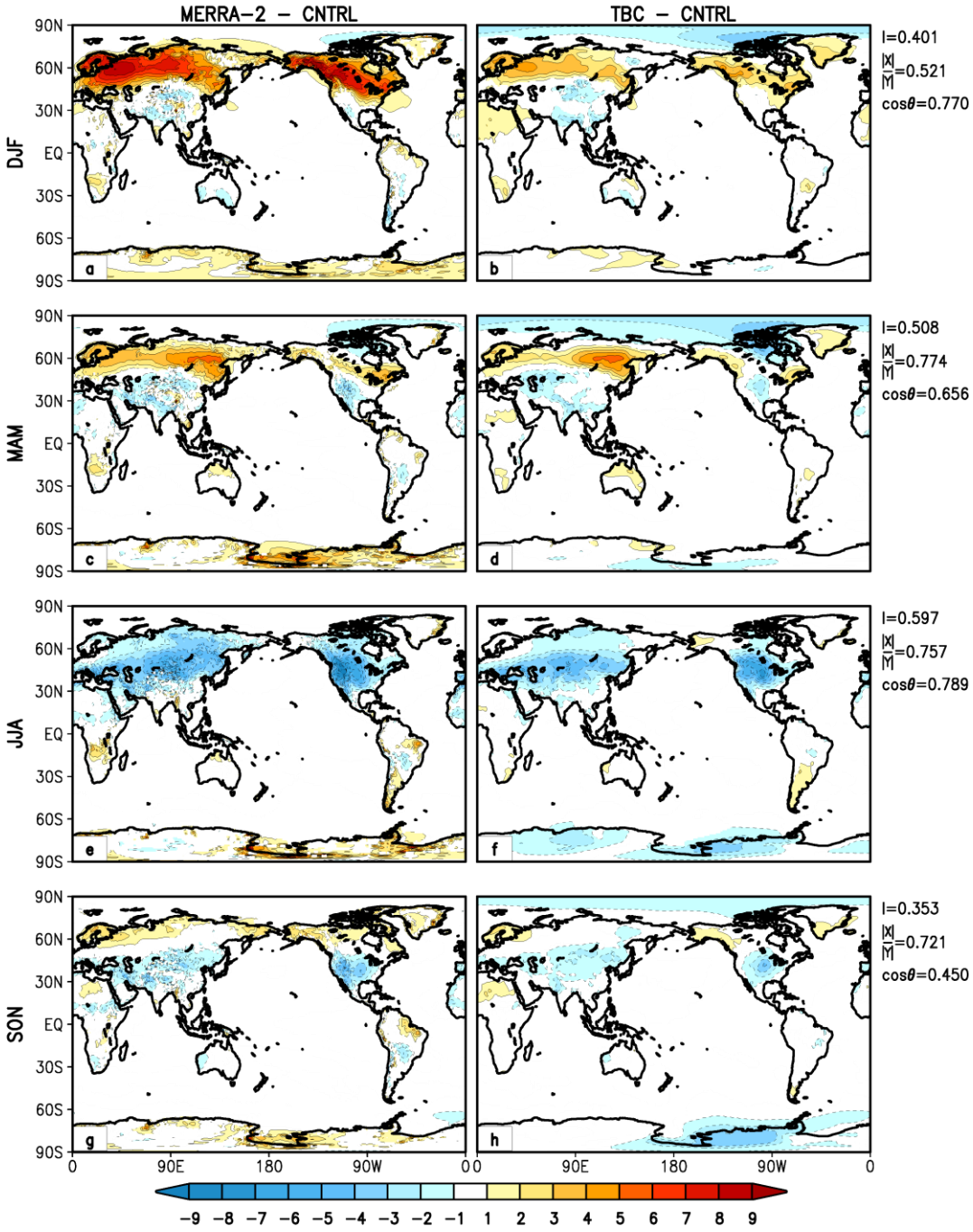

Figure 5: Results for T2m for each season. The left panels are negative of the bias (MERRA-2 - CNTRL) and the right panels are the impact of the TBC (TBC_GLOBAL minus CNTRL). Values are averaged over the period 1980-2017. Units are °C.

u-wind, in that most of the correction to T2m that occurs in the NM zonal band (again, only over the land areas) is due to the TBC applied just in the NM zonal band. The bottom row of Figure 6 shows the contributions of the TBC applied to each of the six NM subregions to the impact seen over the NM_5 (North America) region from TBC in the NM region. While the NM_2 region is again an important contributor during JJA (Fig. 6g) and SON (Fig. 6h), contributing roughly 30% of the total impact, that is not the case for DJF (Fig. 6e) and MAM (Fig. 6f). In fact, during DJF the main contributor to the impact over the NM_5 region is local (the TBC applied to the NM_5 region alone). During MAM, both the upstream (NM_4) and local (NM_5) regions play a role, while for both JJA and SON the three regions NM_2, NM_4 and NM_5 all roughly contribute the same amount (one third) to the impacts over the NM_5 region.

Turning to Table 3, we examine in more detail the T2m bias correction that occurs over North America (the NM_5 region). Here again, two numbers are shown (separated by dashed lines) corresponding to two different validation products used to compute the bias (MERRA-2 on the left and ERA-5 on the right). Focusing on the second column of Table 3, we see that the percent of the bias in region NM_5 corrected by TBC applied to the NM zonal band accounts for about 62% for JJA, 43% for SON, 29% for DJF, and 26% for MAM, with some mostly minor differences between the results for the two different validation products. In the above, we have averaged the two values computed from the two different validation products. The relatively low percent of bias correction during DJF is largely a reflection of a weak amplitude of the correction (the spatial similarity is 0.86). In contrast, the relatively small bias correction for MAM is more a reflection of a relatively weak spatial similarity, equal to 0.57. It is noteworthy that the percent of the T2m bias in the NM region corrected by TBC is, for all seasons, slightly larger when using ERA5 for validation. Why

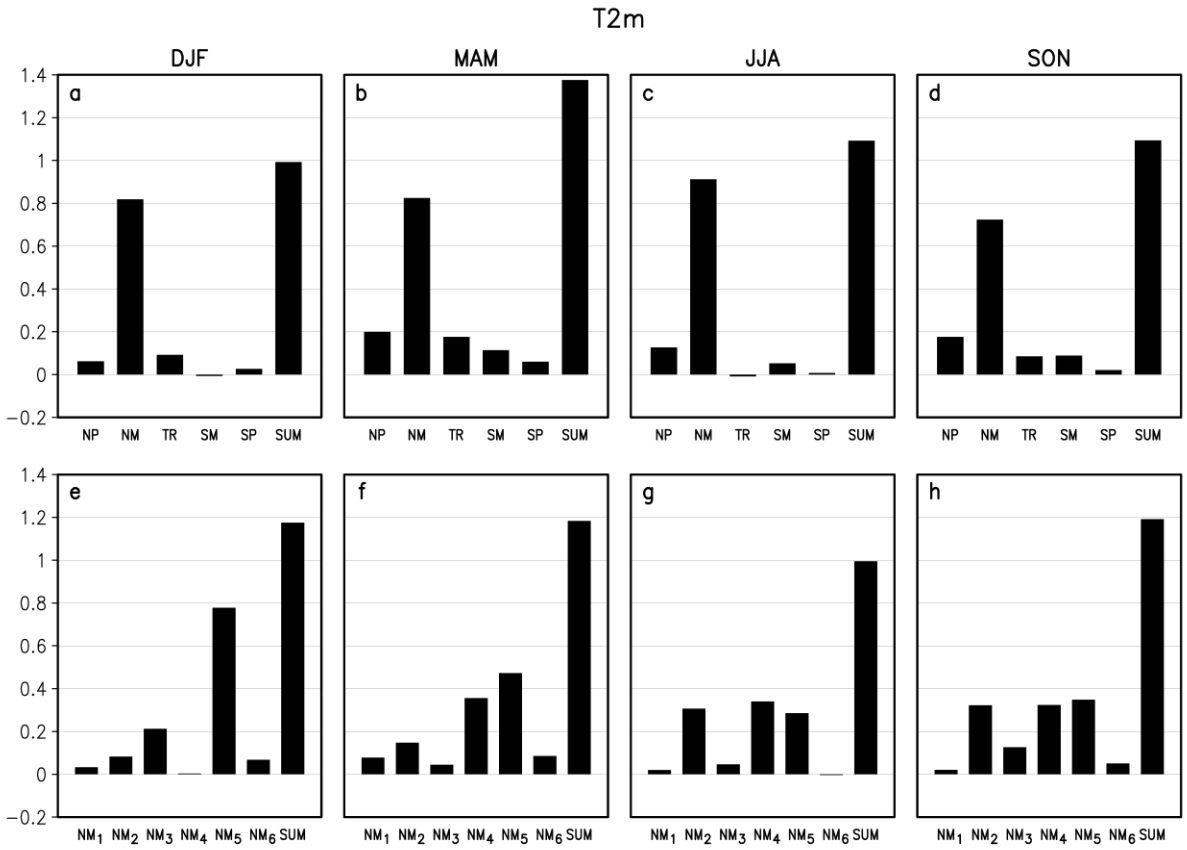

Figure 6: Top panels: The contributions for each season to the global TBC impacts on T2m in the NM region from TBC in each of the zonal band subregions (NP, NM, TR, SM, SP). The last bar in each plot is the sum of the contributions from each zonal band. Bottom panels: The contributions for each season to the NM TBC impacts in the NM_5 (North American) region from each subregion of NM (NM_1, NM_2, NM_3, NM_4, NM_5, NM_6). The last bar in each plot is the sum of the contributions from each subregion of NM. The values are the normalized inner products as defined in eq. 3 of the text. See Figure 2 for the definitions of the regions.

that should be the case is unclear. Overall, the results indicate that TBC appears to be more effective in reducing the T2m bias during the summer and fall seasons, and less effective during the winter and spring seasons. The third, fourth and fifth columns of Table 3 show the contributions to the corrections in the NM_5 region from TBC applied to regions NM_2, NM_4 and NM_5, respectively. The

results highlight the importance of the TBC applied locally during all seasons (accounting for between 20% - 25% of the correction in each season). In fact, during DJF and MAM it is all local (NM_5), consistent with what we saw for the DJF impacts (Fig. 6e). This is not the case for MAM which, while showing some impacts on the NM_5 region from the TBC in the NM_4 region (Fig. 6f), produces essentially no bias correction from that region (Table 3, bottom cell of fourth column). This highlights the fact that impacts do not necessarily translate into actual bias corrections. Both JJA and SON have contributions from all three regions, with JJA having roughly three equal contributions, and SON having NM_2 and NM_4 contributions that are roughly half of the local contribution. As such, for JJA the corrections to the bias in the NM_5 region are roughly 2/3 remote and 1/3 local, while for SON, it is roughly ½ remote and ½ local.

Table 3. The bias correction for the M2_AGCM for T2m in the NM_5 (North American) region for TBC applied in the NM region (second column) and the contributions from the NM_2 (third column), NM_4 (fourth column), and NM_5 (fifth column) subregions, as well as the sum of the corrections from all 6 NM subregions (last column). The results show the decomposition of the inner product (in black, as a percent) in terms of an amplitude ratio (in blue, as a percent) and spatial similarity (in red) as defined by the RHS of equation 3 in the text. For the values to the left of the dashed lines, the biases are computed with respect to MERRA-2, and the values to the right of the dashed lines are the same except that the biases are computed with respect to ERA-5. See Fig. 2 for the definitions of the regions.

Season	bias corrected from TBC in NM region:		from TBC in NM_2		from TBC in NM_4		from TBC in NM_5		SUM	
JJA	**58.4**	**65.9**	**16.8**	**19.0**	**19.8**	**22.2**	**17.2**	**19.9**	**58.5**	**66.2**
	63.1	70.3	20.9	23.4	23.9	26.6	25.4	28.7	66.8	74.7
	0.92	0.94	0.80	0.81	0.83	0.83	0.67	0.69	0.88	0.89
SON	**40.9**	**44.8**	**9.9**	**10.3**	**12.3**	**13.4**	**19.5**	**22.4**	**51.5**	**57.7**
	51.4	55.6	23.9	25.8	22.8	24.6	28.2	31.5	76.3	83.3
	0.79	0.81	0.41	0.40	0.54	0.54	0.69	0.71	0.68	0.69
DJF	**27.9**	**29.6**	**-0.5**	**-0.3**	**-2.6**	**-2.5**	**23.2**	**24.7**	**24.0**	**26.2**
	32.2	34.9	10.3	10.9	11.8	12.4	27.8	29.8	53.7	57.9
	0.87	0.85	-.05	-.03	-.22	-.20	0.84	0.83	0.45	0.45
MAM	**24.3**	**27.7**	**2.4**	**2.1**	**0.9**	**1.5**	**19.5**	**22.7**	**8.3**	**13.4**
	44.3	47.7	13.4	14.4	24.6	26.3	29.6	33.0	82.2	89.3
	0.55	0.58	0.18	0.14	0.04	0.06	0.66	0.69	0.10	0.15

c) Precipitation

Figure 7 is the same as Figure 3, but for precipitation. The model has rather substantial precipitation biases throughout the tropics during all seasons (left panels of Fig. 7). During JJA (Fig. 7e), excessive precipitation extends from the central tropical Pacific into the northern subtropical Pacific, while there is too little precipitation over the warm pool region and over the eastern tropical Indian Ocean. The DJF (Fig. 7a) tropical biases have a north/south dipole structure with too much precipitation north of the equator and too little south of the equator, especially over the Indian Ocean region. Other biases prevalent during all seasons include excessive precipitation over southeast Asia (though less so for DJF, Fig. 7a), northern South America extending south over the Andes Mountains, and much of Central America and surrounding regions, extending into the Atlantic. The model also produces too little precipitation over the central U.S. during the summer (Fig. 7e), and too little precipitation in the North Pacific storm tracks during all but the winter season (though there is a precipitation deficit in the northeast Pacific during that season, Fig. 7a). Global TBC acts to correct some of these biases, though not to same extent that we saw previously for the 250mb u-wind or even for T2m. Here the percent of the global precipitation bias that is corrected with global TBC is 27%, 24%, 30%, and 22%, for DJF, MAM, JJA and SON, respectively (see values in the right margin of Fig. 7). The spatial similarity is generally low, ranging from 0.36 in MAM to 0.50 for JJA. The amplitude ratios are 68%, 67%, 60%, and 57%, for DJF, MAM, JJA and SON, respectively. As such, the overall low values of the percent precipitation bias corrections reflect both a smaller spatial similarity and a weaker amplitude ratio compared to the results for T2m and 250mb u-wind.

Turning next to Figure 8, we show how much the TBC applied separately to each of the different zonal bands contributes to the precipitation impacts in the NM zonal band from global TBC. The results are again quite similar to what we saw for the 250mb u-wind, in that most of the correction to precipitation that occurs in the NM zonal band is due to the TBC applied just in the NM zonal band. Only DJF (Fig. 8a) and SON (Fig. 8d) show some contribution from the tropics (greater than 0.2). There is also considerable double counting especially for MAM (Fig. 8b) and SON (Fig. 8d), for which the SUM is substantially larger than 1 (values are about 1.4 for both). The bottom row of Figure 8 shows the contributions of the TBC applied to each of the six NM subregions to the impact on precipitation over the NM_5 (North America) region from TBC in the NM region. Here we see less of a predominant impact of the NM_2 region, with the other regions (especially the just-upstream NM_4 and local NM_5 regions) contributing as much if not more to the impact over North America. Again, DJF (Fig. 8e) is somewhat of an outlier, with the largest contributions coming from the local (NM_5) and downstream (NM_6) regions. Here again there is also considerable double counting for all but JJA (Fig. 8g), especially for DJF for which the SUM is greater than 2.

Turning now to Table 4, we examine in more detail the precipitation bias correction that occurs over North America (the NM_5 region). Here again, two numbers are shown (separated by a dashed line) corresponding to two different validation products used to compute the bias (MERRA-2 on the left and ERA-5 on the right). Focusing on the second column of Table 4, we see that the percent of the bias in region NM_5 corrected by TBC (I, the values in black) applied to the NM zonal band accounts for about 55% for JJA, 38% for SON, 15% for DJF, and 23% for MAM (here again we are averaging the two values computed from the two different validation products). This highlights the large

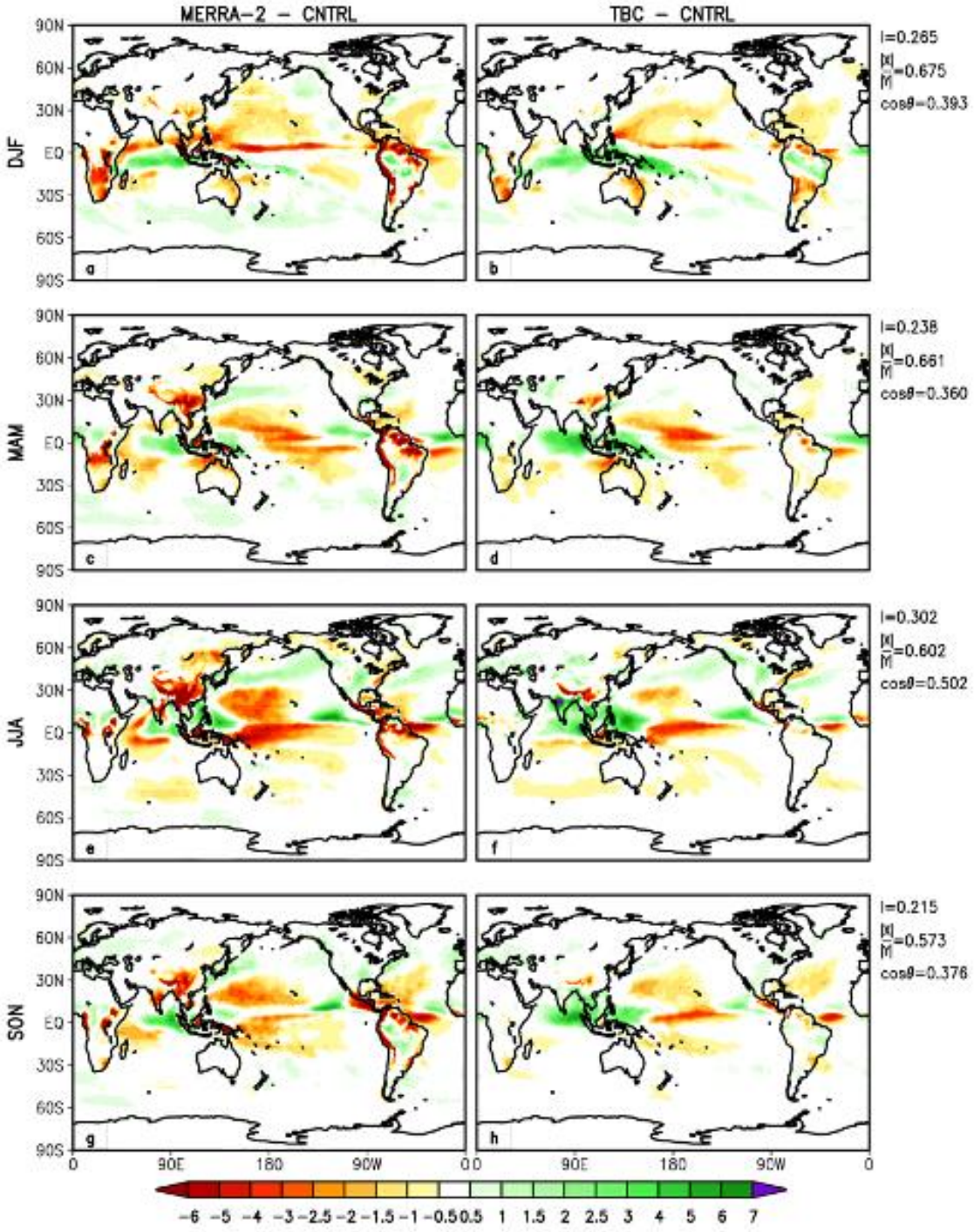

Figure 7: Results for precipitation for each season. The left panels are the negative of the bias (MERRA-2 - CNTRL) and the right panels are the impact of the TBC (TBC_GLOBAL minus CNTRL). Values are averaged over the period 1980-2017. Units are mm/day.

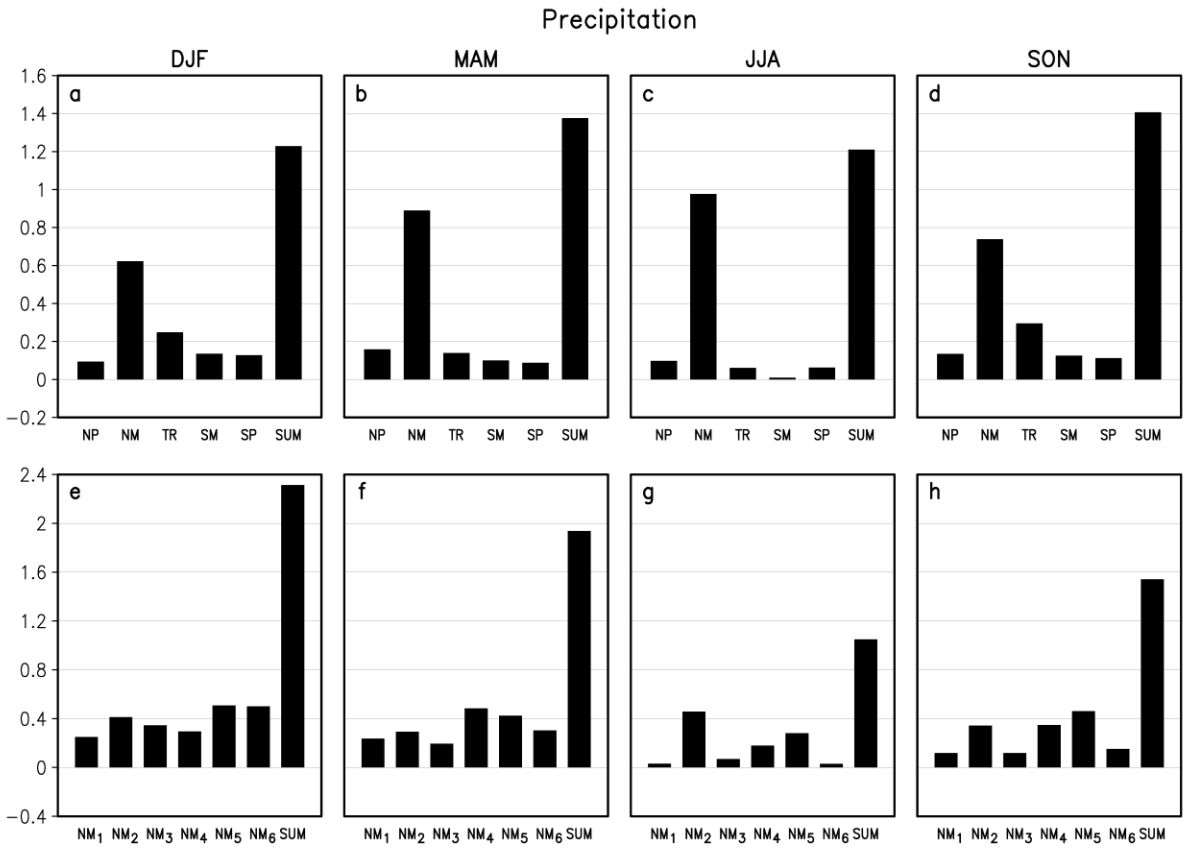

Figure 8: Top panels: The contributions for each season to the global TBC impacts on precipitation in the NM region from TBC in each of the zonal band subregions (NP, NM, TR, SM, SP). The last bar in each plot is the sum of the contributions from each zonal band. Bottom panels: The contributions to the NM TBC impacts in the NM_5 (North American) region from each subregion of NM (NM_1, NM_2, NM_3, NM_4, NM_5, NM_6). The last bar in each plot is the sum of the contributions from each subregion of NM. The values are the normalized inner products as defined in eq. 3 of the text. See Figure 2 for the definitions of the regions.

seasonal differences in the corrections, with JJA exhibiting the largest bias correction, and DJF exhibiting the smallest. We note that in this case there are more substantial differences between the results for the two different validation products (MERRA-2 and ERA-5) compared with the winds and temperature, reflecting the greater uncertainties in our observational estimates of precipitation,

though again the percent corrected is larger when using ERA-5 as validation. Turning to columns 3, 4 and 5 of Table 4, we see that both JJA and SON exhibit relatively large local contributions (NM_5, about 25%), with JJA also showing a relatively large contribution from NM_2 (more than 21%), while SON also shows a relatively large contribution from the upstream region (NM_4, about 23%). For all but JJA, there is again considerable double counting as reflected in the SUM (Last column of Table 4).

The T2m and precipitation bias corrections over North America (the NM_5 region) are summarized in Figure 9 for JJA and DJF – the two seasons that show the largest differences in the amount of bias correction obtained from TBC. The results are shown for the impact of the full NM region (left most bars), the NM_2, NM_4 and NM_5 regions, and the SUM of all 6 regions (right most bars). Here the two bars for each region again correspond to two different validation datasets, one being ERA-5 (for both T2m and precipitation) and the other being the GHCN_CAMS station dataset (for T2m) or the GPCP V2.3 station dataset (for precipitation). For T2m over North America (top panels of Fig. 9), the results highlight the substantial differences between JJA (Fig. 9a) and DJF (Fig. 9b) in terms of the percent corrected as well as the type of correction, with about double the total correction in JJA (60% for JJA versus 30% for DJF), and with 2/3 of the JJA correction coming from remote regions (NM_2 and NM_4) and 1/3 local (NM_5). In contrast, during DJF essentially the entire correction is local (NM_5). For precipitation (bottom panels of Fig. 9), the results again highlight the substantial differences between JJA (Fig. 9c) and DJF (Fig. 9d) in terms of the percent corrected as well as the type of correction, with almost a factor of 4 larger total correction in JJA (55% for JJA versus 15% for DJF), and with 1/2 of the JJA correction coming from remote regions (NM_2 and NM_4) and 1/2 local (NM_5). Interestingly, none of the precipitation bias correction during DJF is

local (NM_5), with both the NM_2 and NM_4 contributing to what is admittedly a relatively small total correction coming from the TBC in the NM region. We note again that there is substantial double counting for DJF (the SUM is considerably larger than the results for NM), suggesting again that some caution needs to be taken when interpreting the results from the individual subregions of NM.

Table 4. The bias correction for the M2_AGCM for precipitation in the NM_5 (North American) region for TBC applied in the NM region (second column) and the contributions from the NM_2 (third column), NM_4 (fourth column), and NM_5 (fifth column) subregions, as well as the sum of the corrections from all 6 NM subregions (last column). The results show the decomposition of the inner product (in black, as a percent) in terms of an amplitude ratio (in blue, as a percent) and spatial similarity (in red) as defined by the RHS of equation 3 in the text. For the values to the left of the dashed lines, the biases are computed with respect to MERRA-2, and the values to the right of the dashed lines are the same except that the biases are computed with respect to ERA-5. See Fig. 2 for the definitions of the regions.

Season	bias corrected from TBC in NM region:		from TBC in NM_2		from TBC in NM_4		from TBC in NM_5		SUM	
JJA	**49.5**	**60.5**	**17.2**	**25.5**	**7.8**	**11.5**	**27.8**	**27.4**	**62.9**	**77.7**
	91.3	94.4	59.6	61.6	37.0	38.2	60.0	62.0	142.6	147.4
	0.54	0.64	0.29	0.41	0.21	0.30	0.46	0.44	0.44	0.53
SON	**35.8**	**40.3**	**4.9**	**8.0**	**21.6**	**25.3**	**24.8**	**25.4**	**70.2**	**82.2**
	63.9	70.2	42.5	46.6	45.1	49.6	49.6	54.4	156.0	171.3
	0.56	0.57	0.11	0.17	0.48	0.51	0.50	0.47	0.45	0.48
DJF	**13.1**	**16.8**	**7.3**	**8.1**	**9.5**	**13.7**	**-1.5**	**-1.4**	**37.3**	**55.3**
	65.3	67.9	46.3	48.2	41.9	43.5	56.3	58.5	212.3	220.6
	0.20	0.25	0.16	0.17	0.23	0.31	-0.03	-0.02	0.18	0.25
MAM	**17.8**	**27.5**	**8.4**	**11.3**	**10.1**	**15.0**	**7.4**	**10.5**	**45.9**	**60.8**
	49.3	55.6	30.3	34.1	36.2	40.1	34.3	38.6	154.1	173.7
	0.36	0.49	0.28	0.33	0.28	0.37	0.22	0.27	0.30	0.35

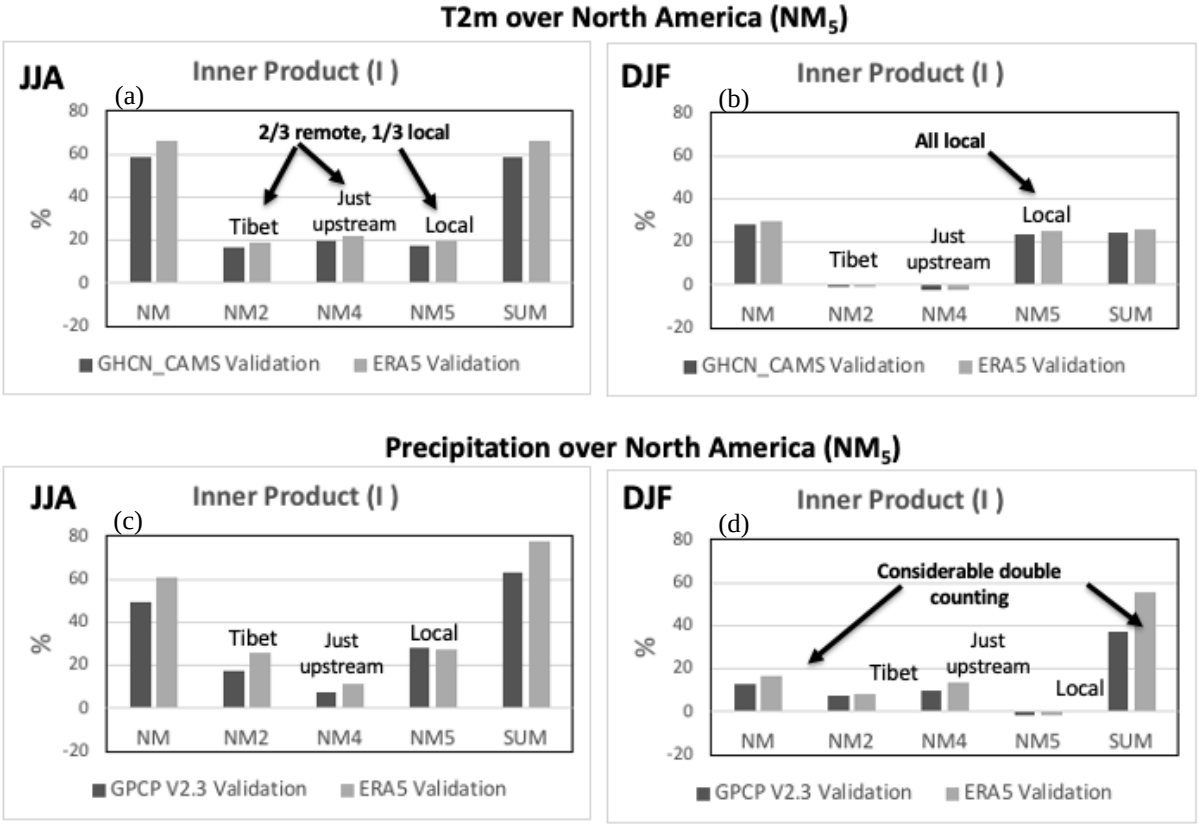

Figure 9: T2m bias correction in NM_5 from TBC in various NM Subregions. The contributions from the NM region and from the NM_2, NM_4, and NM_5 subregions, as well as the sum of the corrections from all 6 NM subregions, are shown. The biases are computed with respect to station observations (dark bars) or ERA-5 (light bars). The values are the normalized inner products as defined in eq. 3 of the text. See Figure 2 for the definitions of the regions.

3.2 Corrections to other diagnostic fields

It is unclear exactly how the constant short-term corrections (the TBCs) introduced in the various prognostic equations (for temperature, winds, humidity, surface pressure and ozone) lead to the improvements in the long-term climate biases. Are the improvements the result of realistic changes in the underlying physics and dynamics terms, or are they the result of adjustments to those fields that are inconsistent with the framework of the existing parameterizations (Fig. 10)? In other words, could the tendency corrections be producing the right answers for the wrong reasons? An example is if TBC introduces a correction in the u-wind equation to correct a wind bias, when in fact the error responsible for the wind bias is in the model's temperature equation.

We examine that question here by looking further into the impacts on quantities not directly corrected by the TBCs. In particular, we examine the impacts on the cloudiness and the surface fluxes over land (latent heat, sensible heat, long-wave and short-wave radiation). To the extent that these are corrected, it gives us some confidence that the corrections are driven by the improved inputs to these physical parameterizations. In the next four figures (one for each season) and for each quantity, the left panels again show the negative of the climate bias (with respect to MERRA-2), while the right panels show the impact (global TBC minus CNTRL). While ideally, we would want to compare the impacts of TBC with independent observational estimates, we argue that our target here should really be MERRA-2, since it is unlikely that we can do better than that within the constraints imposed by the underlying model used to produce MERRA-2. The success of the TBC in correcting the biases is again measured in terms of the inner product (3). We focus in particular on the measure of *similarity in the patterns* of the biases and the TBC impacts ($\cos\theta$), since that is

perhaps the most telling measure of whether or not TBC (by modifying the prognostic fields – the input to the relevant physical parameterizations) is acting in a physically realistic way to correct the biases, even if the amplitude of the correction is insufficient to fully correct the biases (amplitude ratio is substantially less than 1).

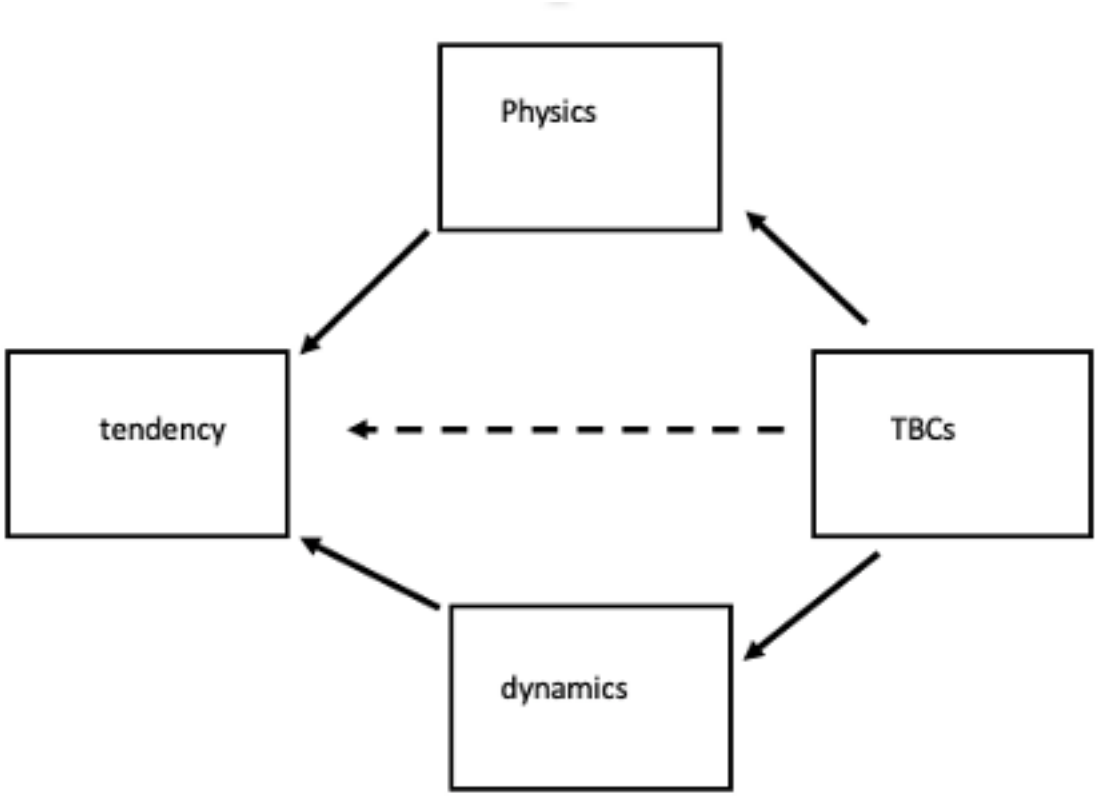

Figure 10: Schematic of how the TBCs might be acting to influence the tendencies. This could be indirectly through the impacts on the physics and dynamics terms (solid arrows), or directly (dashed arrow).

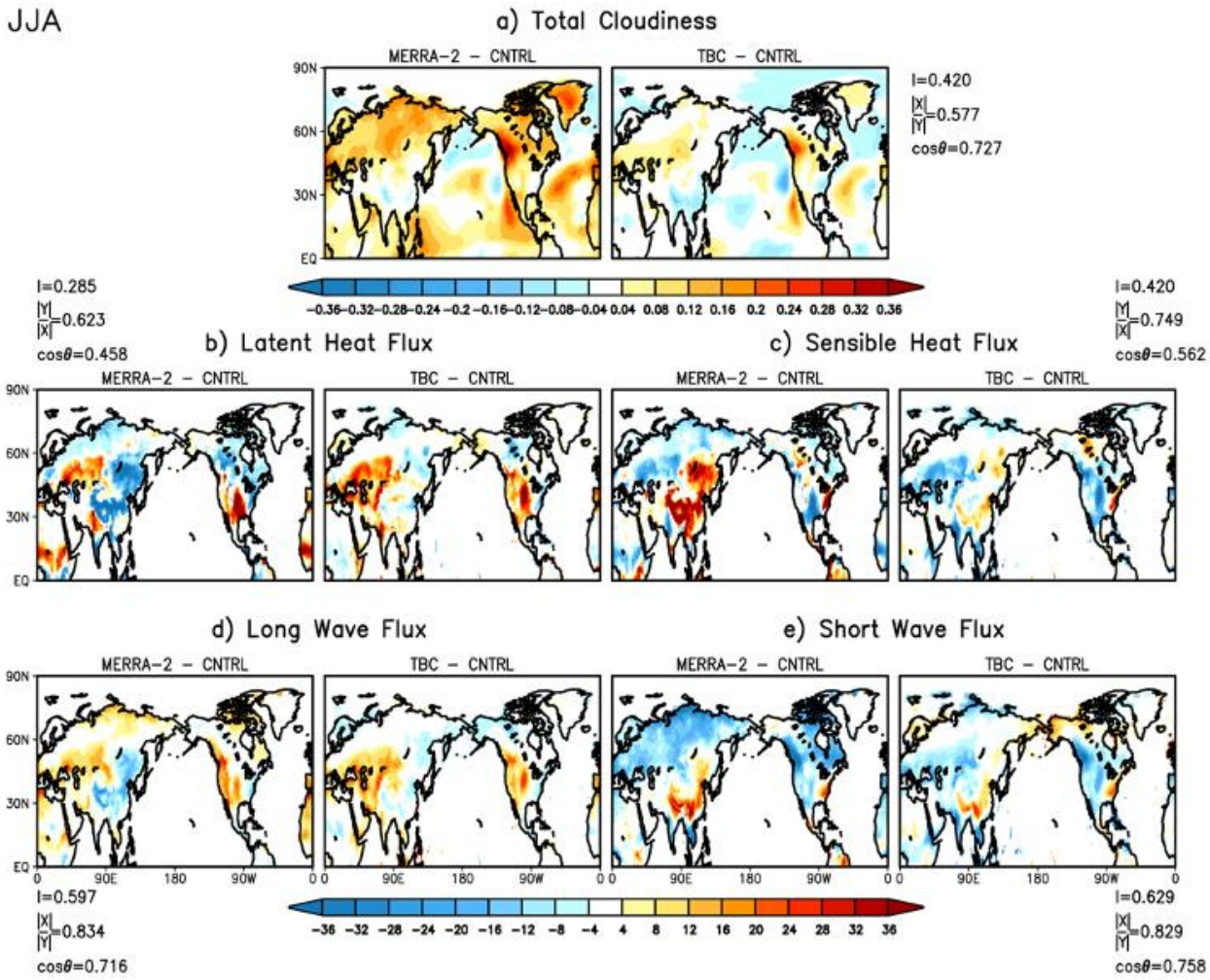

Figure 11: Impacts for JJA of global TBC on a) total cloudiness (fraction of area), b) latent heat flux, c) sensible heat flux, d) longwave flux at the surface and, e) shortwave flux at the surface. In each set of two panels the left panel is the negative of the bias (MERRA-2 minus CNTRL), and the right panel is TBC minus CNTRL. Values are averaged over the period 1980-2017. Units are: W/m^2.

Figure 11a shows the impacts on the total cloudiness in the Northern Hemisphere during JJA. Here we see that the general spatial pattern of the corrections do indeed act to correct the cloudiness biases ($\cos\theta$ = 0.73), though the amplitude of the corrections are too small (amplitude ratio = 0.58) especially in those regions where the CNTRL model has too little cloudiness (the positive values in

the left panel of Fig. 11a). Nevertheless, focusing on North America and the surrounding regions we see that the TBC does an overall good job of acting to correct the cloudiness biases. The TBC is less effective in reducing the overall biases in the latent (Fig. 11b, $\cos\theta = 0.46$) and sensible (Fig. 11c, $\cos\theta = 0.56$) heat fluxes, though it seems to do better if we just focus on North America. It is especially effective in reducing the negative latent heat flux bias and positive sensible heat flux bias over the central U.S. and northern Mexico, presumably as a result of the reduction of the precipitation bias there. The TBC is least effective in correcting the large latent and sensible heat flux biases that occur over much of China. The TBC does an overall good job of reducing the biases in the longwave (Fig. 11d, $\cos\theta = 0.72$) and shortwave (Fig. 11e, $\cos\theta = 0.76$) radiation fluxes. Again, the TBC performs especially well over North America. It also does well over much of Asia south of about 60°N, with the lack of improvement in the surface radiative fluxes over northern Eurasia presumably reflecting the small impact on the cloudiness biases there (Fig. 11a).

The results for SON are shown in Figure 12. Here we see that the CNTRL model produces insufficient cloudiness over much of the Northern Hemisphere (left panel of Fig. 12a; recall that the plot shows the negative of the bias), especially over the extratropical land areas. The impact of TBC is overall weaker than for JJA. The impacts on cloudiness have roughly the right spatial distribution ($\cos\theta = 0.60$) but they are too small to substantially correct the cloudiness biases, especially those over northern Eurasia and North America. The TBC does correct some of the latent (Fig. 12b, $\cos\theta = 0.45$) and sensible (Fig. 12c, $\cos\theta = 0.48$) heat flux biases, though again the overall corrections are weak (I = 0.27 for latent, and 0.32 for sensible). Similar to JJA, the TBC is nevertheless effective in reducing the negative latent heat flux bias and positive sensible heat flux bias over the central U.S. and northern Mexico, though it is less effective in correcting the relatively large latent and

sensible heat flux biases that occur over much of China during SON. Despite the overall weak impact of TBC on the cloudiness, the TBC does a reasonable job of correcting the longwave (Fig. 12d, $\cos\theta = 0.67$) and shortwave (Fig. 12e, $\cos\theta = 0.69$) flux biases over southern Eurasia and parts of North America.

TBC does little to correct the cloudiness biases for DJF, which are primarily characterized by insufficient cloudiness over northern Eurasia and Canada (Figure 13a, $\cos\theta = 0.09$). In fact, the main impacts of TBC occur in the tropics and are, in some places, of the wrong sign. Similarly, there is little impact of TBC on the latent heat (Fig. 13b, $\cos\theta = 0.11$) and sensible heat (Fig. 13c, $\cos\theta = 0.28$) fluxes though, somewhat surprisingly, the TBC impacts on longwave (Fig. 13d, $\cos\theta = 0.34$), and shortwave (Fig. 13e, $\cos\theta = 0.70$) fluxes are in fact acting to reduce the biases (though it should be noted that, with the exception of the region encompassing southeast Asia, these biases tend to be relatively small). These results are overall consistent with what we've already seen in Section 3.1: TBC seems to be less effective in correcting climate biases during DJF compared with the other seasons.

Figure 14 shows the impact of TBC for MAM. The cloudiness biases (Figure 14a) are similar to those for DJF (overall insufficient cloudiness over Eurasia and North America), and the impacts of TBC are again rather small. Nevertheless, TBC acts to produce some improvement in the cloudiness ($\cos\theta = 0.51$) especially over southern Eurasia, China, and western North America, and these are reflected in improvements in the longwave (Fig. 14d, $\cos\theta = 0.65$) and shortwave flux biases (Fig. 14e, $\cos\theta = 0.73$). We also see some improvements in the latent (Fig. 14b, $\cos\theta = 0.36$) and sensible (Fig. 14c, $\cos\theta = 0.34$) heat flux biases, especially over Eurasia.

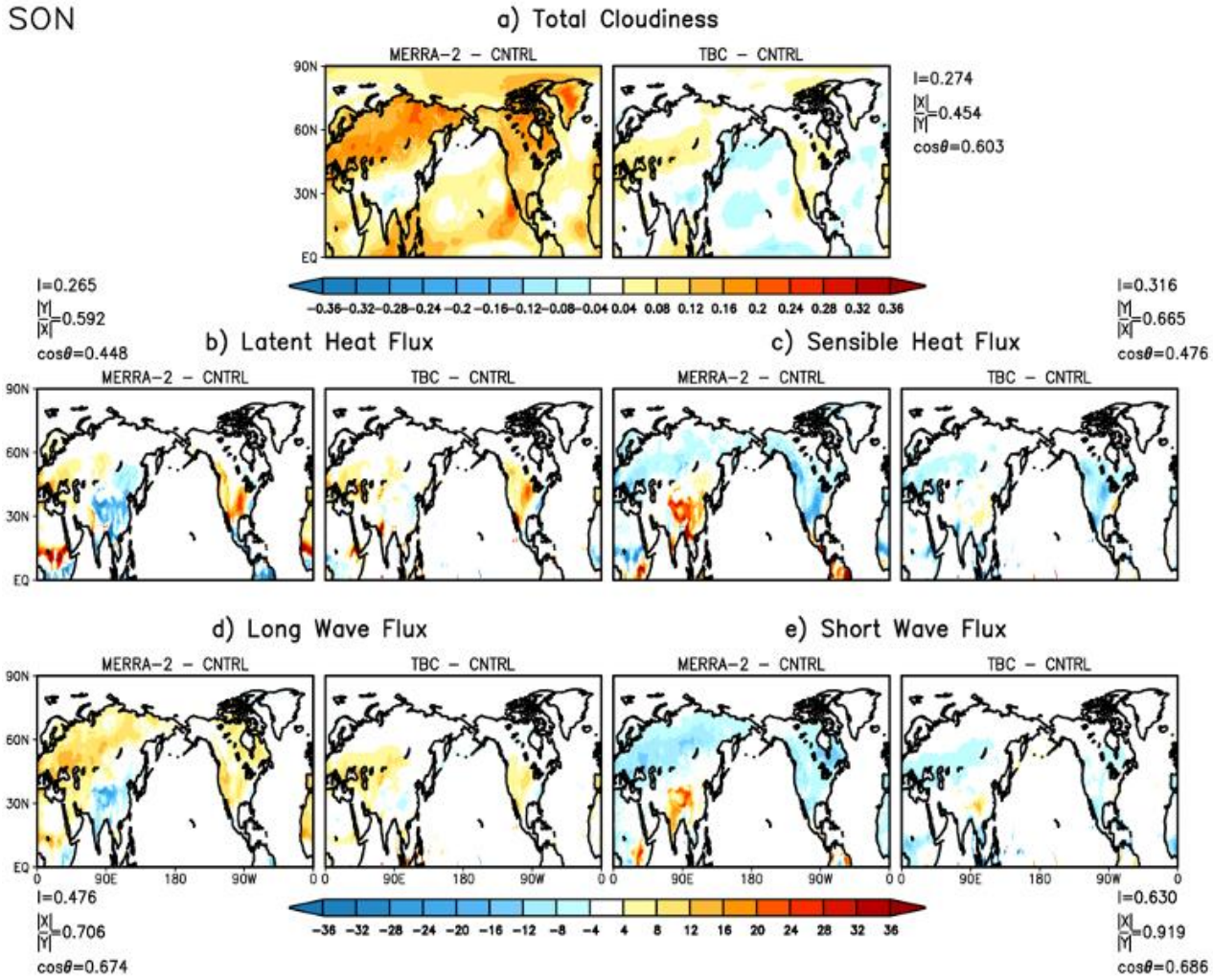

Figure 12: Impacts for SON of global TBC on a) total cloudiness (fraction of area), b) latent heat flux, c) sensible heat flux, d) longwave flux at the surface and, e) shortwave flux at the surface. In each set of two panels the left panel is the negative of the bias (MERRA-2 minus CNTRL), and the right panel is TBC minus CNTRL. Values are averaged over the period 1980-2017. Units are: W/m^2.

Overall, we find that the seasonality of the improvements in these diagnostic fields is consistent with that of the various prognostic (and precipitation) fields we already examined in Section 3.1. In

particular, the improvements are greatest for JJA and poorest for DJF, with the transition seasons falling somewhere in between (though SON appears to behave somewhat more like JJA, and MAM

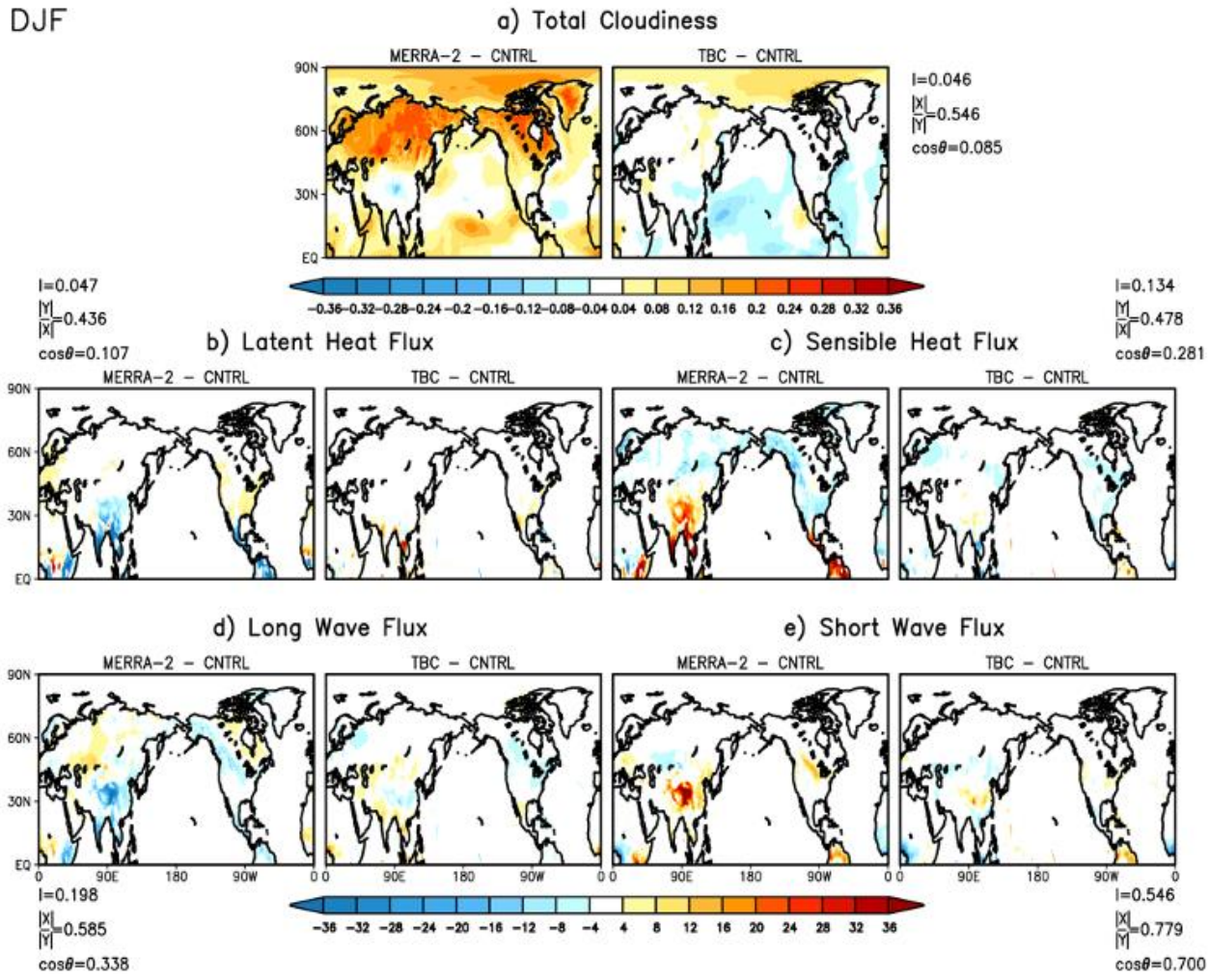

Figure 13: Impacts for DJF of global TBC on a) total cloudiness (fraction of area), b) latent heat flux, c) sensible heat flux, d) longwave flux at the surface and, e) shortwave flux at the surface. In each set of two panels the left panel is the negative of the bias (MERRA-2 minus CNTRL), and the right panel is TBC minus CNTRL. Values are averaged over the period 1980-2017. Units are: W/m^2.

more like DJF). As such, we believe that the improvements we see in the climate biases, particularly for the warm season, do reflect (at least in part) the fact that the various physical parameterizations

are benefiting from improved input fields, and so the climate bias corrections we see are being made in a physically realistic manner (see discussion at the beginning of this section).

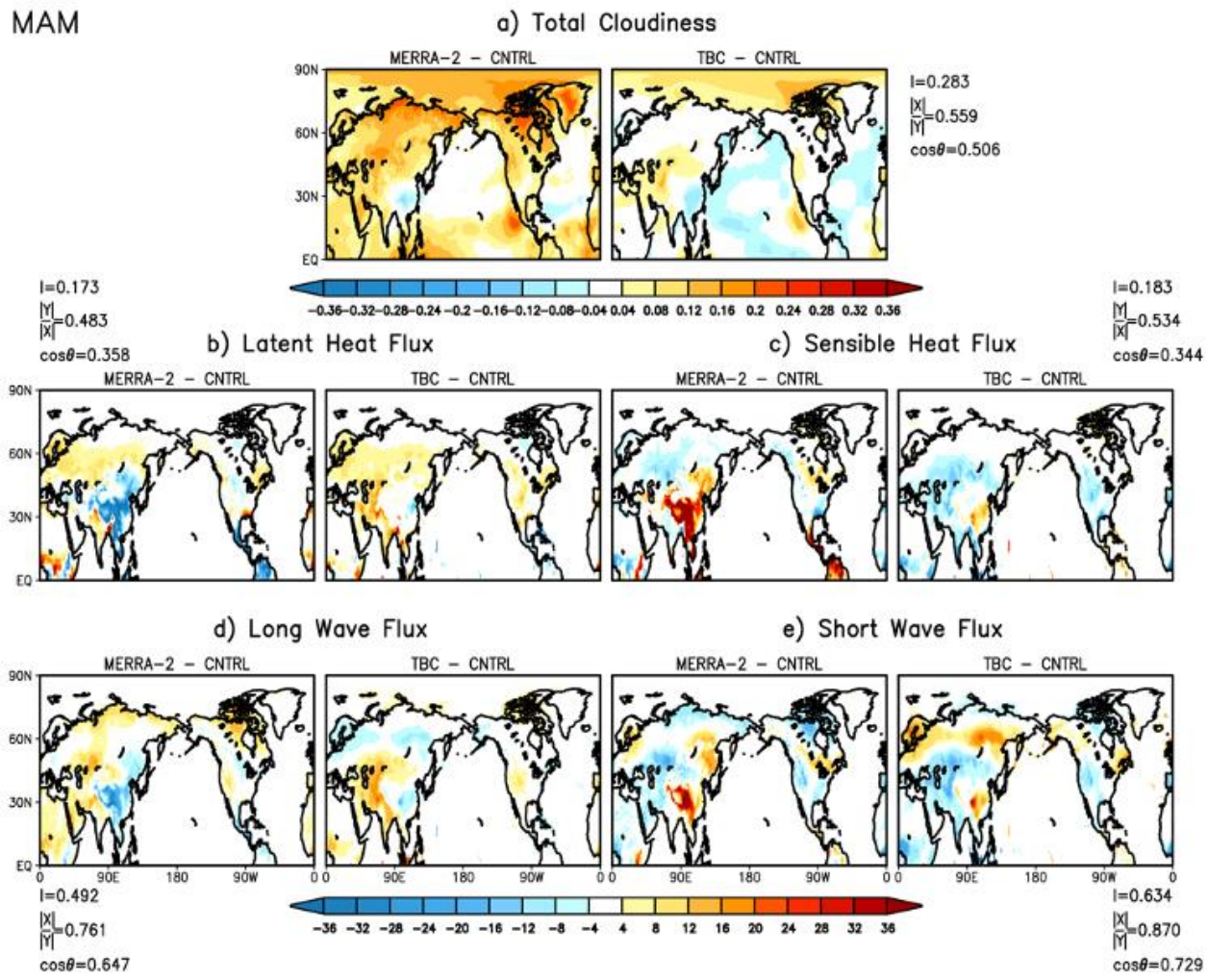

Figure 14: Impacts for MAM of global TBC on a) total cloudiness (fraction of area), b) latent heat flux, c) sensible heat flux, d) longwave flux at the surface and, e) shortwave flux at the surface. In each set of two panels the left panel is the negative of the bias (MERRA-2 minus CNTRL), and the right panel is TBC minus CNTRL. Values are averaged over the period 1980-2017. Units are: W/m^2.

3.3 A closer look at the boreal winter stationary waves

While the previous results show that TBC is overall effective in correcting many of the long-term climate biases of the M2_AGCM, it is least effective for the boreal winter hemisphere (e.g., Fig. 3 and Fig. 9). The problem is especially evident for the stationary wave biases in the North Pacific/North American region (cf. the top panels of Fig. 15), which have a negative PNA-like (Wallace and Gutzler 1981) structure, a problem that has persisted in the GEOS AGCM over many generations of the model. While TBC does not correct those NH biases, we see that it does a much better job of correcting the Southern Hemisphere (austral summer) biases, suggesting that we need to look further into the nature of (and potential biases in) the forcing and propagation of the boreal winter stationary waves.

We begin by looking at a more recent version of the GEOS AGCM (the IC_AGCM; see section 2.2). As already mentioned, negative PNA-like stationary wave biases have persisted over recent generations of the GEOS AGCM, and we see here that they are also present in this more recent version of the AGCM (Fig. 15c). Remarkably, in this case the TBC does a much better job of correcting the boreal winter stationary wave biases (cf. bottom panels of Fig. 15). The reasons for this are unclear, but one difference is that here the TBC's were computed through a process called *replay* rather than by simply utilizing the analysis increments from MERRA-2 directly, as was done for all the results presented so far for the M2_ AGCM.

As described in Takacs et al. (2018) and Chang et al. (2019), *replay* takes advantage of the incremental analysis update (IAU) procedure employed in the GEOS data assimilation system to

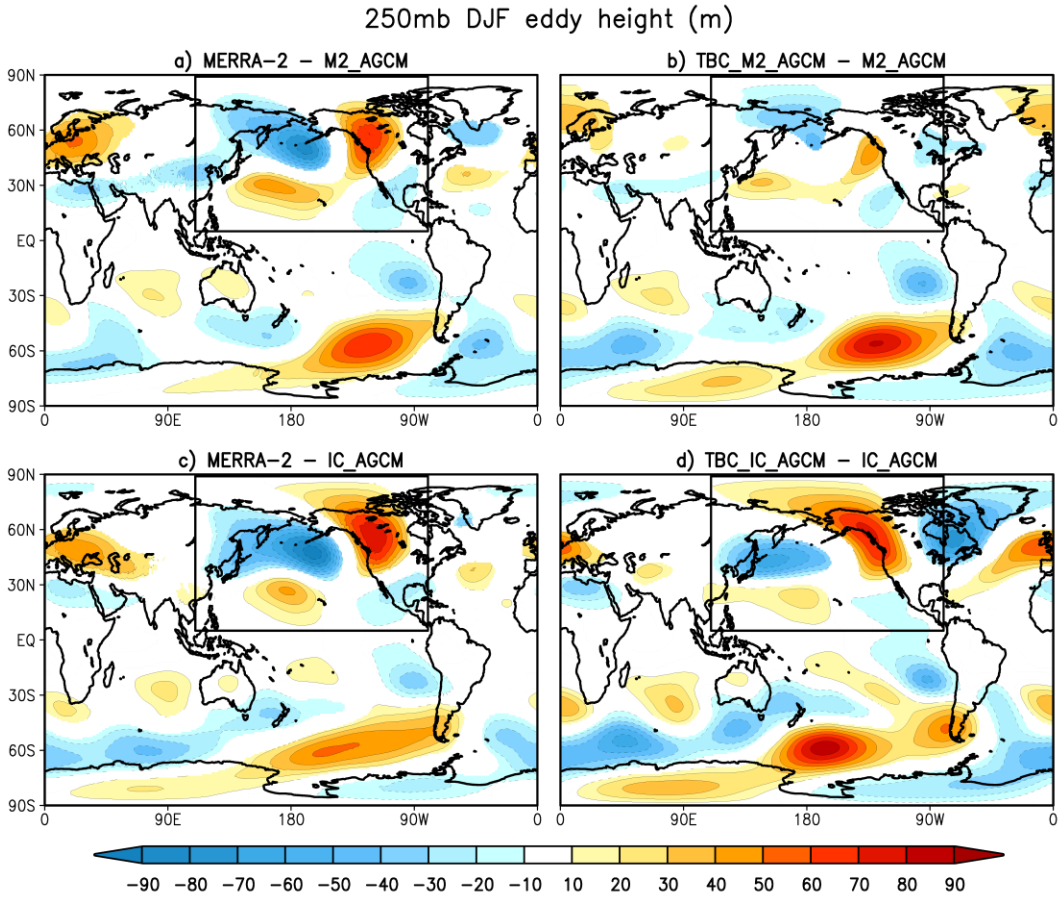

Figure 15: Impact of TBC on the 250mb eddy (deviations from the zonal mean) height field compared to the model bias. The left panels are the negative of the bias with respect to MERRA-2. The right panels show the impact of TBC. The top panels are for the M2_AGCM (averaged for the period 1980-2017). The bottom panels are for the updated model (the IC_AGCM), averaged for the period 1981-2016. Units are meters. The box in each figure outlines our region of interest - the Pacific/North American region.

force a model to track a *pre-existing analysis*. The equations governing replay have the same form as noted earlier for the assimilation (see eq. 1). The difference from the assimilation is that now the analysis used in computing $\triangle x$ is a pre-existing analysis which is simply read in during the course of the integration. The implementation of replay at the GMAO is outlined in Figure 16.

As such, the increments (and the TBCs) from *replay* are a more direct estimate of the tendency biases for that particular model. It should be noted that had we employed the exact same version of the model used to produce MERRA-2 (here we did not, since the model was run at a lower resolution), the *replay* increments ($\triangle x$) would be the same as those obtained from MERRA-2. This, in fact, highlights another key advantage of *replay* – the ability to recreate exactly an existing reanalysis without having to actually redo the analysis with the full data assimilation system.

While it is difficult to pinpoint exactly how the *replay*-based TBCs lead to a better correction of the stationary waves, we suspect it has to do with the extent to which the TBC corrects the tropical precipitation/heating fields. To examine that in more detail in the IC_ AGCM, we next look at the separate contributions to the stationary wave corrections coming from the tropics (TBC_TR) and Northern Hemisphere middle latitudes (TBC_NM). Figure 17 shows the results for the 250mb DJF height anomalies. Here we show the full height anomalies (rather than just the eddy component as we did earlier) to get a better sense of the full impact of TBC, including the zonal mean component. The results show that the TBC_GLOBAL not only does a credible job of correcting the stationary wave biases (as we've already seen in Fig. 15), but also corrects a substantial amount of the overall negative height bias that characterizes the tropics of the CNTRL AGCM (cf. Figs. 17a and b). Figs. 17d and e show the separate impacts of applying TBC in the tropical region (TBC_TR) and the Northern Hemisphere middle latitude region (TBC_NM), respectively. The results suggest that TBC in both the tropics and extratropics appear to play a role in correcting the stationary wave bias, especially the corrections to the ridge over western North America.

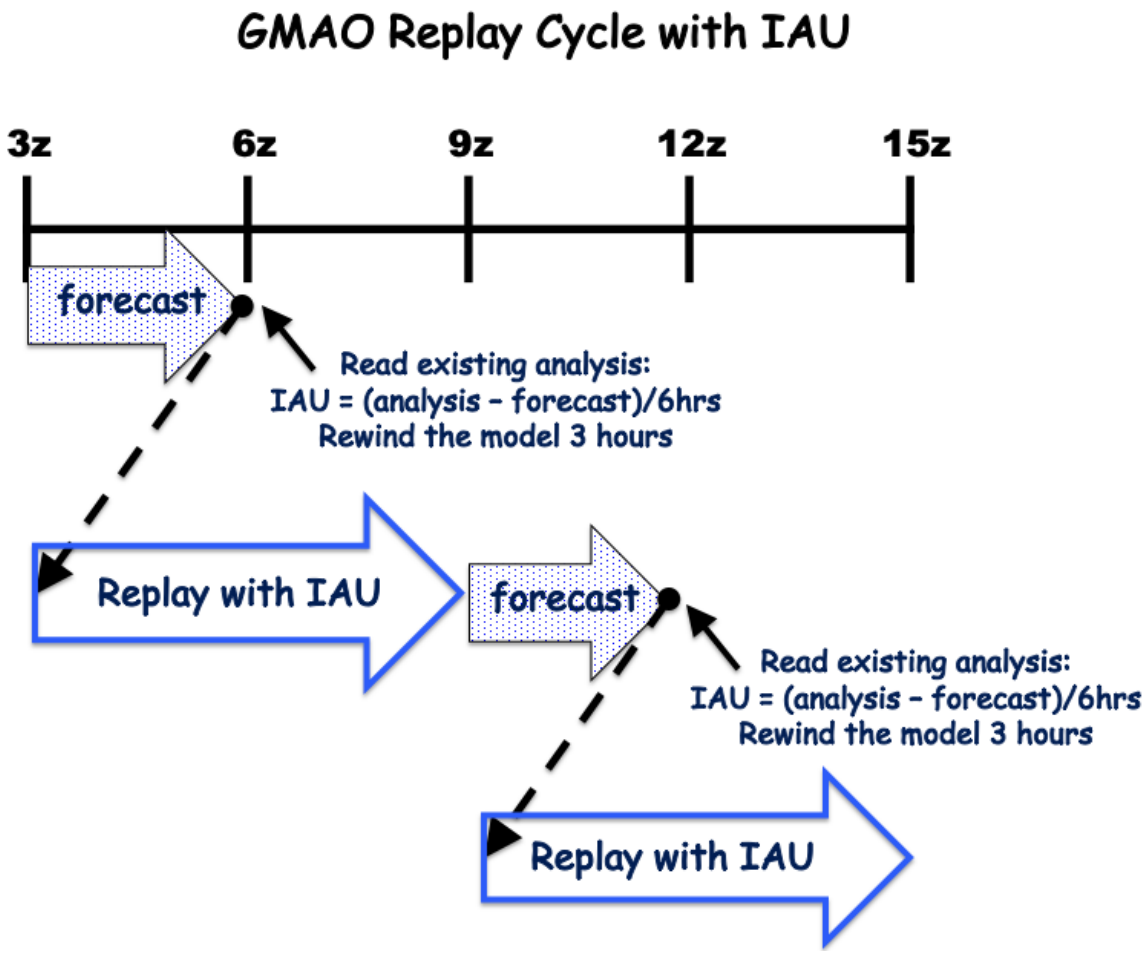

Figure 16: A schematic of the replay approach used to compute the analysis increments (IAU, or Δx in our current terminology) from an existing analysis (figure taken from Chang et al. 2019). Here IAU refers to the incremental analysis update procedure for performing data assimilation developed by Bloom et al. (1996). See also Takacs et al. 2018 for further information about the numerical stability of replay.

A more detailed decomposition of the impact of the TBC_NM run shows that the corrections over North America are primarily from TBC in the TBC_NM_3 and TBC_NM_4 regions (see Fig. 2 for the locations of these regions), with the former located over the jet core, and the latter located just upstream of the North American ridge (results not shown). Given that there is some double counting

in the Pacific/North American region (cf. Fig 17b and 17c), we argue that the key underlying model errors producing the stationary wave biases are located in the tropics. Here we are speculating that TBC in the NM_3 and NM_4 regions is likely correcting jet biases that are in actuality due to errors in

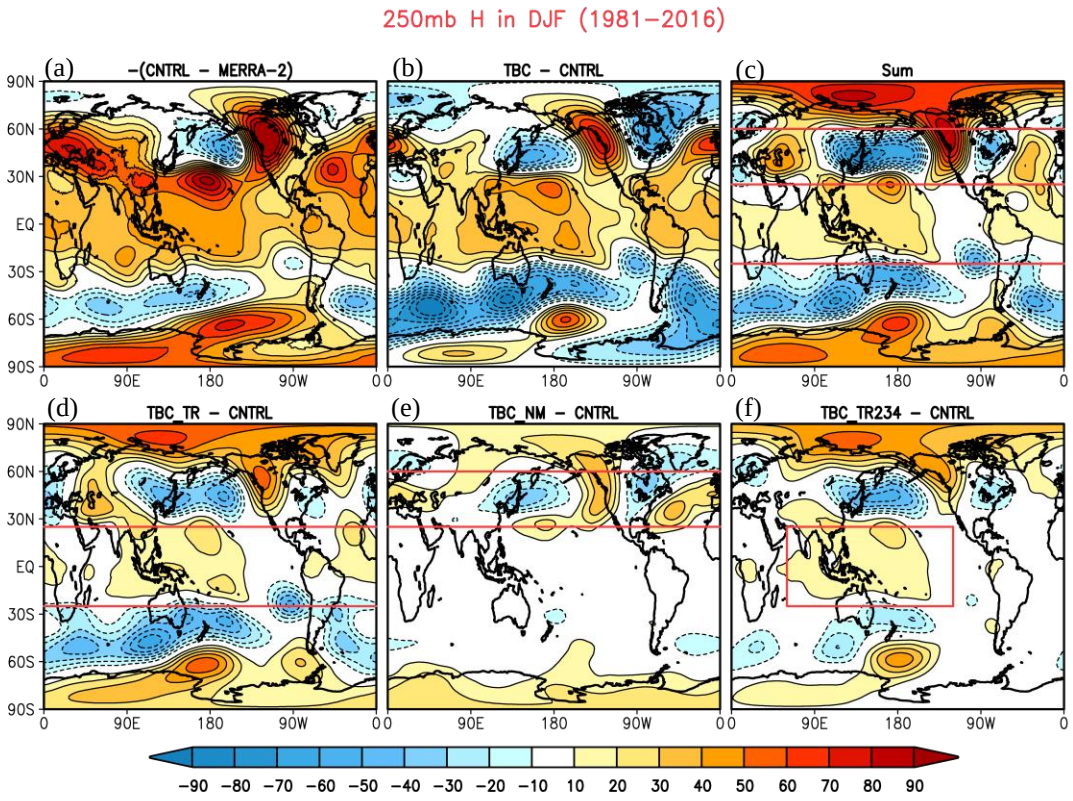

Figure 17: The impact of global and regional TBC on the 250mb height field for the IC_AGCM. a) negative of the bias with respect to MERRA-2, b) the impact of global TBC, c) the sum of the impacts from the tropical (TR) and northern middle latitude (NM) TBC, d) impact of TR TBC, e) impact of NM TBC, f) impact of applying TBC in the region that combines TR_2 and TR_3 and TR_4. Results are averages for the period 1981-2016. Units are meters.

the tropics. Furthermore, Fig.17f shows that applying TBC in the extended tropical subregion (TR_2+TR_3+TR_4) reproduces much of the correction obtained from TBC_TR (cf. 17d and 17f).

We next turn, in Fig. 18, to an examination of the impact on the precipitation in the IC_AGCM. Comparing Figs. 18a and Fig. 7a, we see that overall, the IC_AGCM precipitation biases are quite similar to those for the M2_AGCM. Nevertheless, there are some differences in the details, including the negative biases just south of the equator that extend into the western Indian Ocean region, and the more extensive positive anomalies north of the equator centered over southeast Asia in the M2_AGCM. The TBC_GLOBAL with the IC_AGCM (Fig. 18b) corrects much of the tropical bias, especially over the maritime continent. The main difference with the results for the M2_AGCM (Fig. 7b), is that the TBC_GLOBAL for the M2_ AGCM fails to correct much of the positive precipitation bias north of the equator in the Indian Ocean extending eastward to southeast Asia and appears to overcorrect the negative precipitation biases over a region encompassing the maritime continent and extending southeastward into the SPCZ. Plots of the separate impacts of TBC_TR (Fig. 18d) and TBC_NM (Fig. 18e) in the IC_AGCM show that the former accounts for basically all the precipitation bias corrections made with TBC_GLOBAL. There is overall little impact from TBC_NM other than weak scattered negative corrections throughout the Northern Hemisphere oceans. We already saw in Fig. 17f that the TBC in the $TR_2 + TR_3 + TR_4$ region is key to correcting the stationary wave bias in the PNA region. We now see from Fig. 18f that it is primarily the correction of the east/west dipole in the tropical precipitation bias (negative precipitation bias over the maritime continent and positive bias to the east) that appears to be critical to that improvement.

The above results suggest that improvements to the boreal winter hemisphere stationary waves (in the PNA region) are to a large extent tied to improving the heating fields in the tropics in a region

extending eastward from the eastern Indian Ocean well into the Pacific warm pool region. To the extent the Indian Ocean region plays a role, it is likely that AGCMs with specified SSTs are fundamentally incapable of fully reproducing the observed stationary waves, since in that region atmosphere/ocean coupling appears to be important for obtaining the correct surface fluxes (e.g., Wu and Kirtman, 2004), and so here TBC is likely giving the correct answer for the wrong reason.

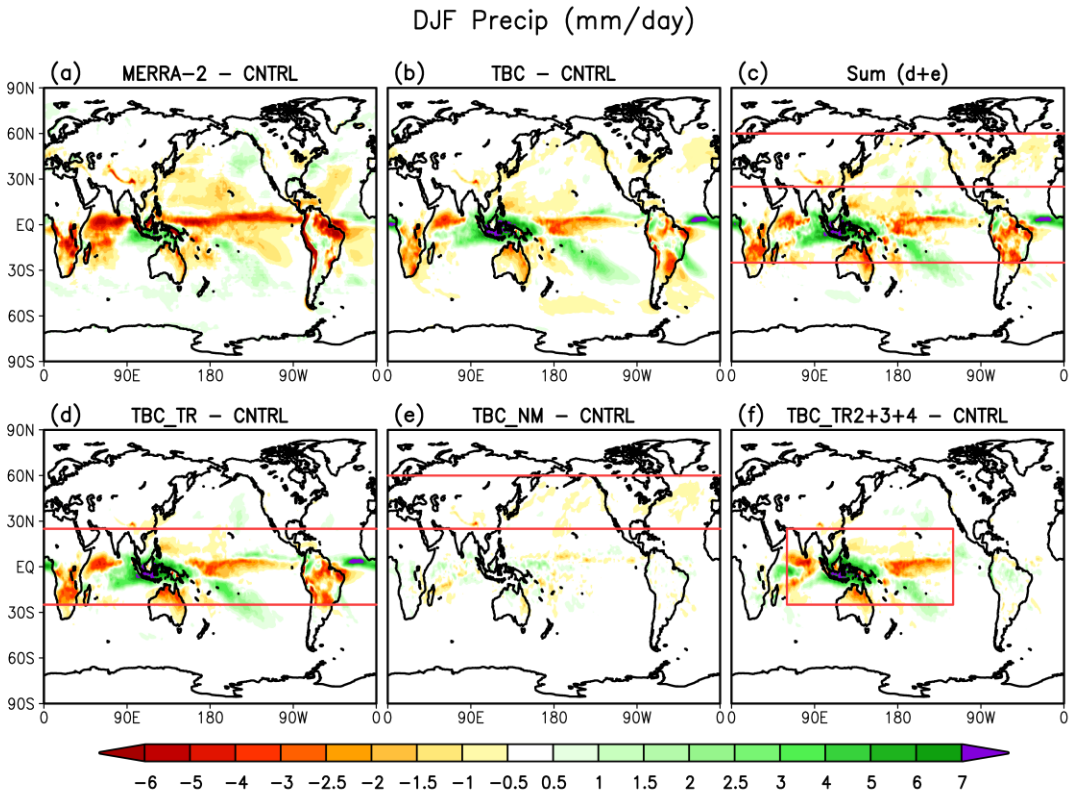

Figure 18: Same as Fig. 17, except for the precipitation. Units are mm/day.

4. Discussion

We next address the question of why TBC appears to be, for the most part, quite successful in correcting many of the GEOS AGCM's long term climate biases. We also examine the limitations of TBC for (when applied globally) bias correction and for (when applied regionally) isolating the regions responsible for the climate biases. This is followed by some ideas and preliminary results on a possible extension to TBC.

4.1 Why does TBC work and its limitations

The underlying idea is that the TBCs (which are based on short-term forecast errors) reflect error growth that is linear and therefore should provide a reasonable estimate of the biases in the model tendencies, subject to any observational/analysis biases (e.g., Xue et al., 2013; Bhargava et al. 2018; Chang et al. 2019). While early generations of the reanalyses suffered from model spin-up and spurious responses to the observations making estimates of the initial tendencies problematic, this has become much less of a problem in the more recent generations of reanalyses, in particular, in MERRA-2 which uses an incremental analysis update (IAU) procedure developed by Bloom et al. (1996).

Given the availability of realistic estimates of the initial tendencies, the question remains as to whether correcting the model tendencies with the TBCs leads to realistic responses in the AGCM. If, for example, the TBCs are very large, it is likely that the model would react to them in unexpected and unrealistic ways, similar to the data insertion problems faced by the early reanalyses (e.g., Bloom et al. 1996). As such, we need to examine how large the TBCs are relative to the "physical" terms in

the model's tendency equations. To do that, we look here at the long-term mean of the various terms in the equations (the budget) governing the MERRA-2 assimilation (i.e., the long-term average of eq. 1):

$$\frac{\partial \bar{x}}{\partial t} = \overline{f(x)} + \overline{\triangle x} \approx 0. \qquad (5)$$

As an example, Figure 19 shows the budget terms (5) for the JJA temperature at 850mb (averaged over the years 1980-2016), with the various terms (radiation, moist physics, dynamics, etc.) governing the model's temperature tendency shown in the top six panels. The magnitudes of those terms in many places typically exceed 2°C/day with maximum values locally exceeding 5°C/day. Of course, on an instantaneous basis, these terms are very likely to achieve magnitudes considerably larger than that. We note that the friction term (with magnitudes less than the minimum contour interval shown here, top middle panel of Fig. 19) tends to play a significant role primarily near the surface. The bottom left panel shows that the sum of those 6 terms tends to be substantially smaller (magnitudes less than 1°C/day), reflecting the cancelation between relatively large terms with opposite sign. The bottom middle panel of Fig. 19 shows the average temperature increment (the TBC term) which is, by design, exactly equal and opposite to the sum of the physical terms (bottom right panel shows that the sum of the two terms is indeed zero).

As another example, we show in Figure 20 the budget for the JJA 850mb specific humidity. Here again we see that the physics and dynamics terms (top 3 panels) have substantially larger values than the sum (bottom left panel). On the other hand, in this case the sum does have values locally in the tropics, especially over the eastern Indian Ocean and over the Pacific and Atlantic warm pools, that

rival the model's tendency terms. This indicates that the TBCs account for a significant fraction of the moisture changes in these regions, and we must regard our assumption of linearity (the TBCs as a relatively small correction) with some caution.

Results similar to those shown in Figs. 19 and 20 are found for the other seasons (not shown). Overall, we find that the TBCs tend to provide relatively small corrections to the model equations. Although we need to exercise some caution when it comes to interpreting the responses to the tropical moisture TBCs, which appear to be large enough to potentially lead to spurious responses by the model's convective scheme, our results seem to indicate this is not a significant problem, though this may be due to the fact that the AGCM that we are using here is essentially the same as (or similar to) the model used to produce MERRA-2. Whether this is also true for non-native models (models not used in the production of the reanalysis) remains to be seen.

Coming back to the issue of double counting (see eq. 4), we have obtained rather mixed results. Focusing on the Northern Hemisphere extra-tropics (the NM region, see Figure 2) we have found that there is little double counting during JJA. This appears to reflect that fact that there is little impact from the tropics, and so all the TBC impacts have their sources within the NM region. Furthermore, the separate impacts from the various NM subregions also show little evidence of double counting. This is especially true for the impacts on T2m, though somewhat less so for the impacts on precipitation, which appear to show some nonlinearity (e.g., Fig. 9). That nonlinearity becomes much more acute for the precipitation during DJF (e.g., Fig.9), for which we have found considerable double counting ($R_1 + R_2 + \ldots R_N >> R$), making the interpretation of the results from the various subregions difficult. While the exact cause of the double counting in the Northern Hemisphere extra-

tropics and why it tends to be more severe for the cold season is not clear, we believe a key factor has to do with whether or not the errors in the tropics play a role. As such, TBC applied in the extra-

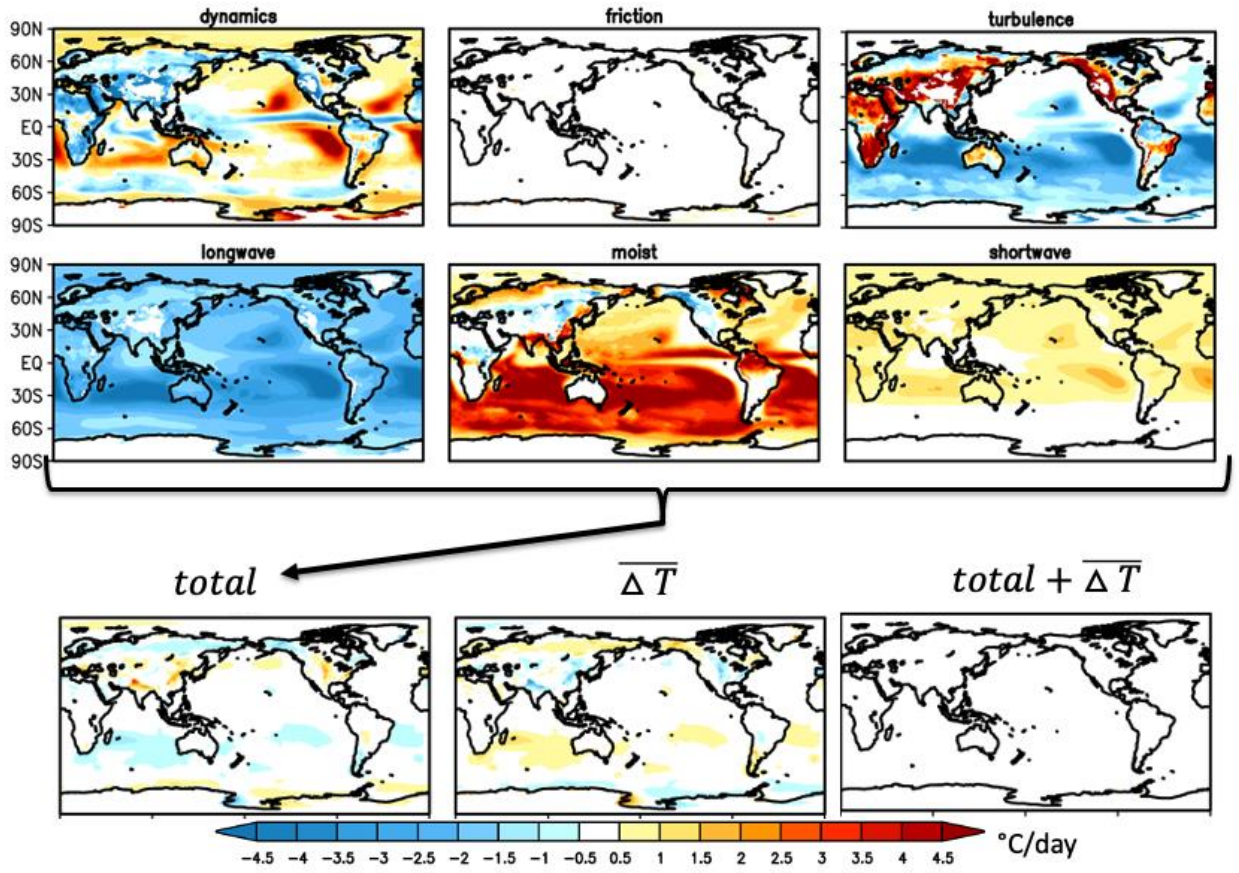

Figure 19: Long term averages (1980-2016, denoted by an overbar) of the various terms of the JJA mean temperature (T) tendency at 850mb computed from MERRA-2. The top 6 panels show the contributions to the tendency from the various physical terms in the thermodynamic equation such that $\frac{\partial \bar{T}}{\partial t} = \overline{dynamics} + \overline{moist} + \cdots + \overline{\Delta T} \cong 0$, where $\overline{\Delta T}$ (lower middle panel) is the long-term average analysis increment of temperature. The lower left panel is the sum (total) of all the physical terms. The lower right panel shows that the long-term average of the sum of the physical terms and the analysis increment is indeed effectively zero. Units: °C/day.

tropics likely applies corrections to tendency biases that in fact have their source in the tropics. The result is an over-correction of the climate biases when the extratropical and tropical impacts are added together.

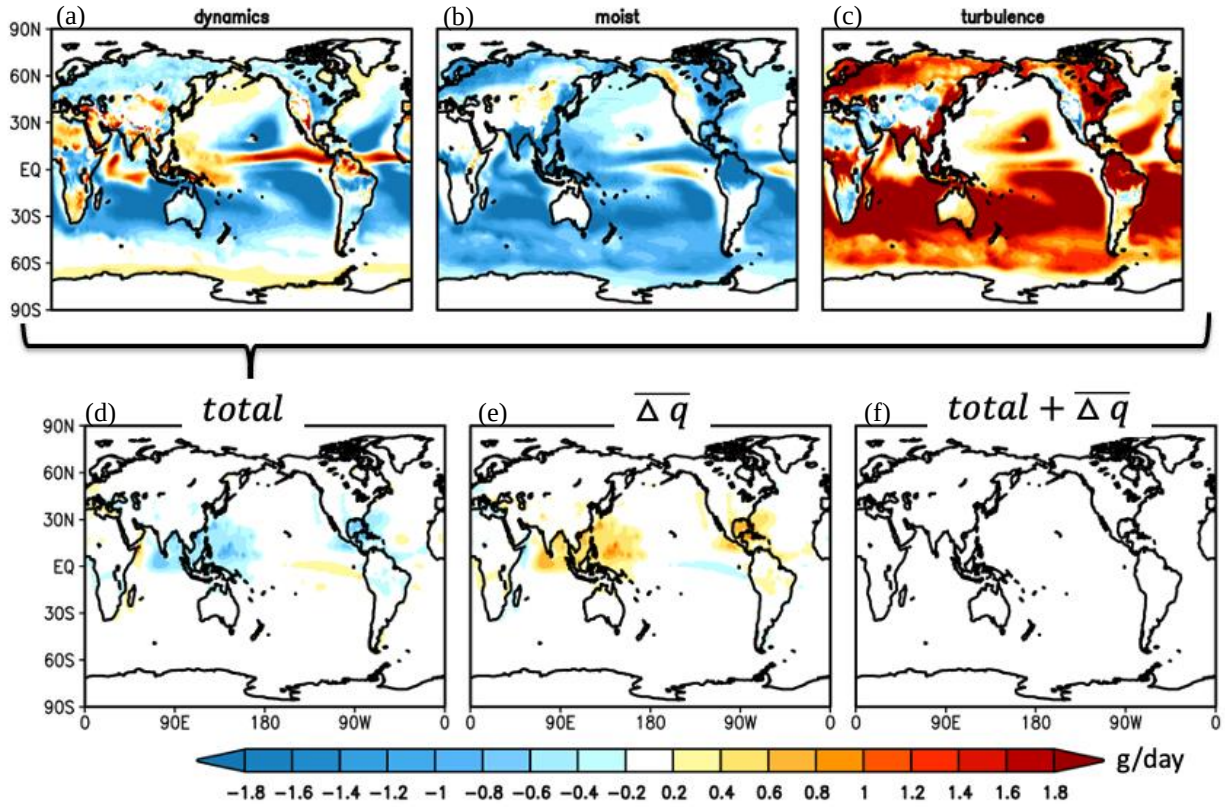

Figure 20: Long term averages (1980-2016, denoted by an overbar) of the various terms of the JJA mean specific humidity (q) tendency at 850mb computed from MERRA-2. The top panels show the contributions to the tendency from the various physical terms in the moisture equation. Here, $\frac{\partial \bar{q}}{\partial t} = \overline{dynamics} + \overline{moist} + \cdots + \overline{\Delta q} \cong 0$, where $\overline{\Delta q}$ (lower middle panel) is the long-term average analysis increment of specific humidity. The lower left panel is the sum (total) of all the physical terms. The lower right panel shows that the long-term average of the sum of the physical terms and the analysis increment is indeed effectively zero. Units are g/day.

4.2 A state-dependent extension of TBC

One of the of the findings of Chang et al. (2019) was that despite the fact that TBC made rather remarkable improvements to the model's climate bias, the impact on forecast skill (both sub-seasonal and seasonal) was modest at best. Here we consider an extension of TBC to include a state-dependent correction term as first suggested by Leith (1978) and recently explored further by Danforth et al. (2007). The basic idea is that such a term more directly corrects time lag covariances, so it could have a more direct impact on forecast skill. In particular, we consider a correction of the form

$$\frac{\partial x}{\partial t} = f(x) + \Delta x, \qquad where\ we\ assume\ \Delta x = \alpha(x - \bar{x}) + \beta. \tag{6}$$

We compute α and β to minimize the tendency error $(\frac{\partial x}{\partial t} - f(x))^2$. We note that if α is set to zero then (6) reduces to the TBC approach ($\beta = \overline{\Delta x}$) described previously (eq. 2).

This work is in progress. An example of α for the surface pressure is given in Figure 21, which shows values that are reasonably smooth in space. Nevertheless, after some experimentation we found it necessary to put a cap on the magnitude of α and to linearly taper the values to zero above 500mb. Some early results of including the state-dependent term (SD-TBC) are presented in Figure 22 for the 850mb u-wind and the 250mb v-wind variance. The results show that there is very little difference in the biases in these fields with the inclusion of the state-dependent term – essentially showing that while these quantities are not improved, we have also done no harm. Similar results are found for other fields including the precipitation (not shown). While there is the possibility of (6) producing a

runaway (unstable) integration depending on the parameter (α), we have so far not faced that situation.

As already mentioned, this is work in progress. Further work should address the issue of statistical significance of the state-dependent term (the αs). Danforth et al. (2007) found that state-dependent corrections resulted in worse prediction skill due to sampling errors in the estimation of the full covariance matrix, though they were able to obtain some improvements by localizing the covariance matrix, or alternatively by introducing an SVD-based formulation of the correction operator.

(a)

(b)

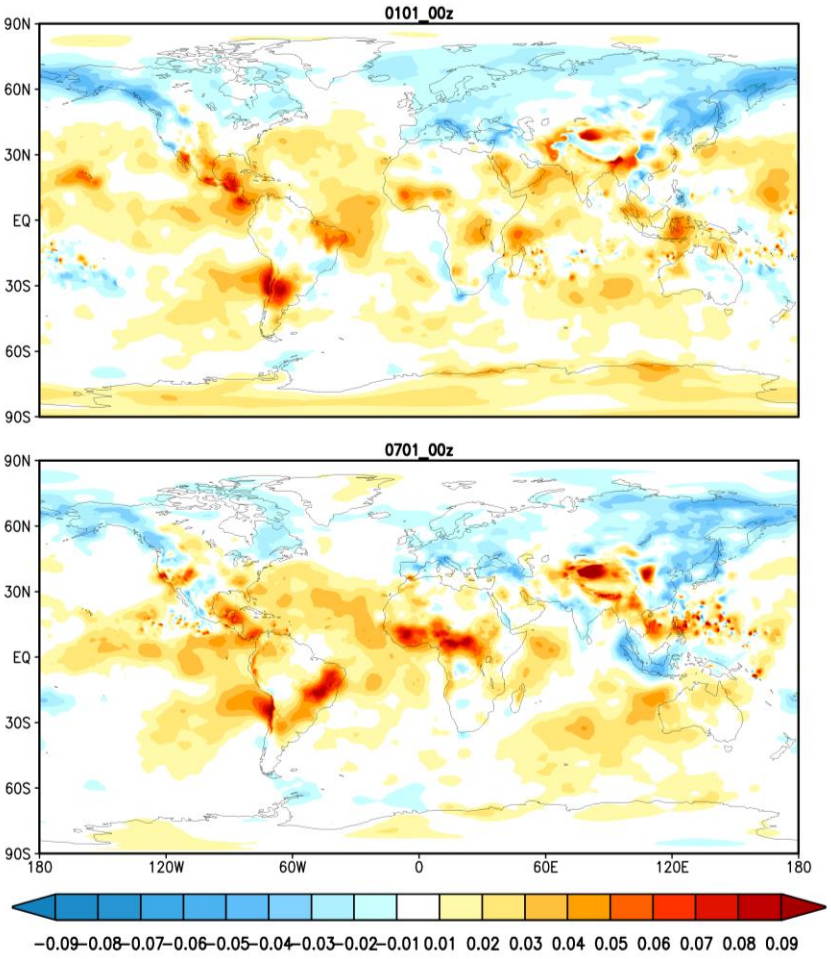

Figure 21: An example of the αs for surface pressure for January and July. Units:1/day

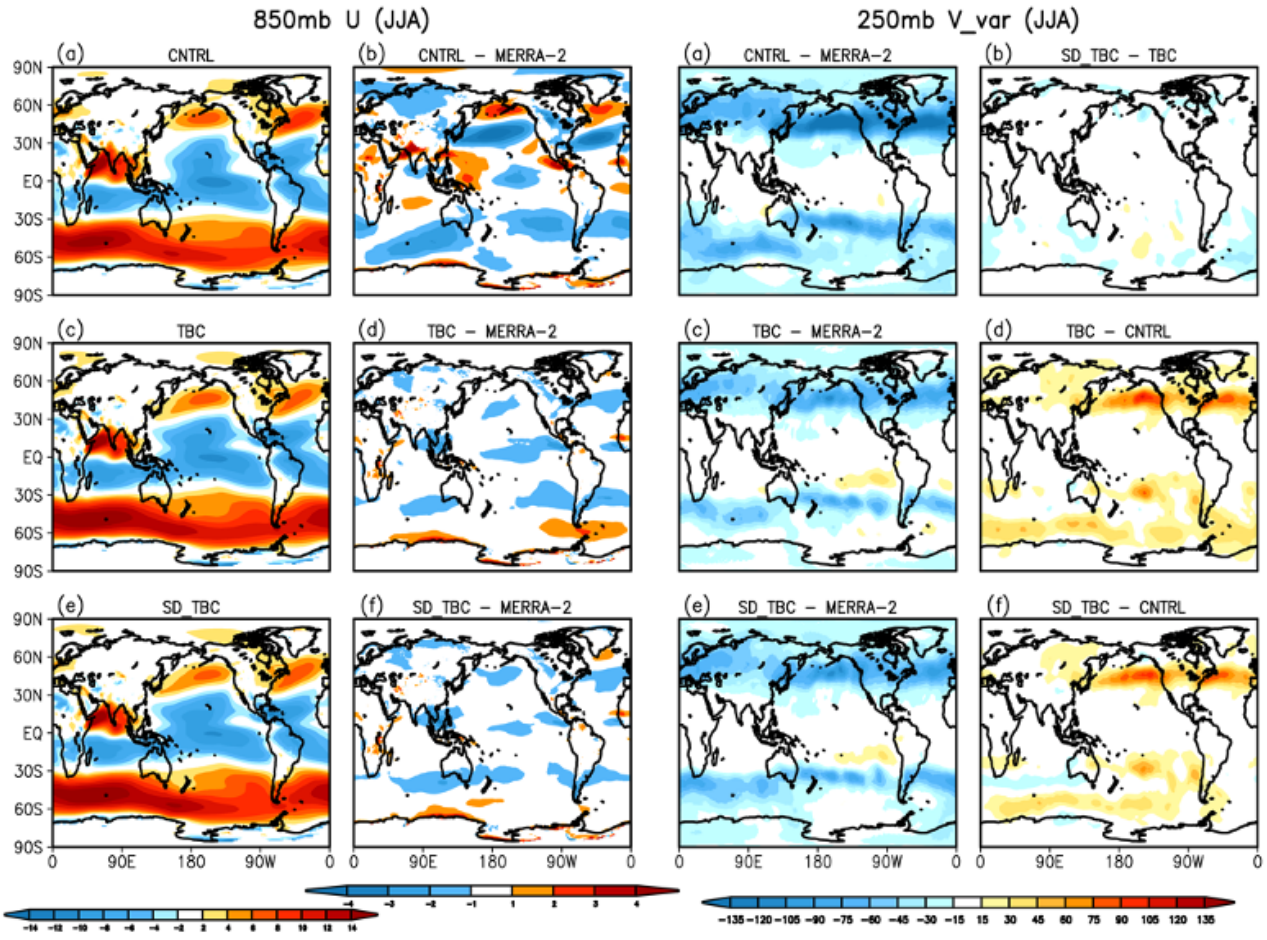

Figure 22: A comparison of the results for TBC and TBC together with a state-dependent term (SD_TBC) for JJA for the 850mb u-wind (m/s, left panels) and the 250mb v-wind variance ((m/s)^2, right panels).

5. Summary and Conclusions

This report extends the work of Chang et al. (2019) and Schubert et al. (2019) by examining in more detail, and more comprehensively, the efficacy of tendency bias correction (TBC) in correcting the GEOS AGCM's long term climate biases. In particular, we have examined the efficacy of TBC as a function of season and looked at the impacts of TBC on additional diagnostic fields. We have also addressed the questions of both why TBC works and what its limitations are, especially when interpreting the impacts of TBC applied regionally. Finally, we have also presented some initial results of an extension to TBC that involves introducing an additional state-dependent term.

TBC, in general terms, involves adding to a model's prognostic equations forcing terms consisting of time averaged short term (typically 6 hour) forecast errors (with opposite sign). For most of the results presented here we have taken advantage of the fact that the AGCM employed here is the same as that used to generate MERRA-2 (though run at a lower resolution) so we have simply taken the history of the analysis increments generated in producing MERRA-2 (coarsened to the model resolution) to calculate the TBCs. The simulations are all forced with observed SST and span the period 1980-2017. Comparisons are made throughout with MERRA-2 as well as with other observational datasets.

Focusing on the Northern Hemisphere middle latitudes (the NM region, see Fig. 2), the results show a substantial seasonality in the efficacy of TBC in correcting many of the long-standing circulation biases (e.g., upper-level jets and stationary waves) of the GEOS AGCM, with the summer season showing the greatest improvements and the winter season showing the least. A key difference between JJA and DJF is the fact that the contributions to the TBC impacts in the NM region in summer tend to be local. That is, the sources of the TBC impacts in NM are largely confined to the middle

latitudes, while during the winter there are substantial contributions to the impacts in NM from other latitude bands, especially from the tropics. The transition season impacts fall somewhere in between, with SON behaving more like JJA, and MAM behaving more like DJF. During all seasons (though less so for DJF) we see an important impact on the climate bias in the NM region coming from the TBC in a region encompassing the Tibetan Plateau, highlighting the importance of correcting the model biases in that very mountainous region.

The results also show a substantial seasonality in the ability of TBC to correct the climate biases in the surface meteorology over North America. For example, during JJA, TBC applied to the Northern Hemisphere middle latitude (NM) region corrects about 60% of the bias in T2m and more than 50% of the bias in precipitation, with roughly 2/3 of that correction coming from TBC applied to remote regions (just upstream and over Tibet) and 1/3 of the correction coming from TBC applied locally (see also Schubert et al. 2019). In contrast, during DJF, TBC applied to the NM region corrects only about 30% of the bias in T2m and less than 20% of the bias in precipitation, with all the correction coming from TBC applied locally.

We have also examined the impact of TBC on other diagnostic fields including total cloudiness and various surface fluxes including the latent and sensible heat fluxes and the longwave and shortwave radiation fluxes. These quantities also show substantial improvements, but again that improvement has a strong seasonality, with the largest improvements occurring for JJA and the smallest improvements occurring during DJF. The improvements in the cloudiness and surface fluxes indicate that the improvements in the climate biases from TBC is, at least in part, the result of improved input (the prognostic quantities) to the various parameterizations, leading to physically realistic improvements to such fields as T2m and precipitation.

While we have found that the TBCs obtained directly from MERRA-2 seem to work quite well in reducing long term climate biases of the M2_ AGCM, they do appear to be suboptimal, especially for correcting the boreal winter stationary waves and related fields. Using an updated GEOS model (IC_AGCM), which has essentially the same circulation biases as the older M2_AGCM, we found that employing a technique called "*replay*" (Takacs et al. 2018; Chang et al. 2019) to generate the TBCs seems to provide improved results, especially during DJF when tendency errors in the tropics play an important role. Furthermore, *replay* has the advantage of allowing any model to be used to track an existing reanalysis, therefore making TBC a viable approach for correcting models not employed in a reanalysis system.

The results with the IC_AGCM show a much stronger impact of TBC during DJF (compared to that for the M2_AGCM) with much improved stationary waves – a result that appears to be due to a much larger impact on the NM region (particularly the Pacific/North American region) from the TBC in the tropics. While the reasons for this are still somewhat unclear, we believe it has to do with the ability of the TBC to correct precipitation errors over a large tropical region encompassing the Indian Ocean and Pacific warm pool – a region where heating anomalies are known to produce Rossby wave responses that have a substantial impact on the extratropics.

We also look more generally at the reasons for why TBC seems to work, looking in particular at the size of the TBCs relative to the physical and dynamical forcing terms in the model. The results show that the TBCs overall tend to be relatively small, suggesting that the model's response to the TBCs is likely linear, though that is less true for the moisture in the tropics where the TBCs can have amplitudes locally that rival those of the physical terms. We in fact do find considerable double

counting when examining the separate impacts of TBC from different regions, and this appears to be especially true for precipitation as well as for DJF, for which the impacts from the tropics are important.

Finally, we present some initial results of an extension to TBC that includes a state-dependent term. The motivation for such an extension is that by minimizing the error in the time tendency, such a term could potentially produce a greater positive impact (compared with TBC) on forecast skill. The results we have obtained so far highlight some of the challenges one faces in producing statistically robust estimates of state-dependent terms and in introducing them in a way that maintains model stability. We are also considering other state-dependent extensions to TBC in which the corrections are conditioned on particular states of the atmospheric/ocean (e.g., the different phases of ENSO). It remains to be seen if the data records (e.g., MERRA-2) are sufficiently long and of high enough quality (especially going back in time) to produce robust corrections for such approaches.

Acknowledgements

This study was supported by NASA MAP funding under NNG17HP01C and WBS 802678.02.17.01.33. MERRA-2 data were developed by the Global Modeling and Assimilation Office (GMAO) at NASA GSFC under funding by the NASA MAP program and disseminated through the Goddard Earth Science Data and Information Services Center (GES DISC). The GEOS model (M2_AGCM and IC_AGCM) simulations were produced by the GMAO.

6. References

Adler, R.F., G.J. Huffman, A. Chang, R. Ferraro, P. Xie, J. Janowiak, B. Rudolf, U. Schneider, S. Curtis, D. Bolvin, A. Gruber, J. Susskind, and P. Arkin, 2003: The Version 2 Global Precipitation Climatology Project (GPCP) Monthly Precipitation Analysis (1979-Present). *J. Hydrometeor*., **4**, 1147-1167**.**

Bacmeister, J. T., and Stephens, G. L., 2011: Spatial statistics of likely convective clouds in CloudSat data, *J. Geophys. Res.,* **116**, D04104, doi:10.1029/2010JD014444.

Bhargava, K., E. Kalnay, J.A. Carton and F. Yang, 2018: Estimation of systematic errors in the GFS using analysis increments. *J. Geophys. Res.: Atmospheres,* **123**, 1626 – 1637. https://doi.org/10.1002/2017JD027423.

Bloom, S. C., Takacs, L. L., da Silva, A. M., & Ledvina, D. (1996). Data Assimilation Using Incremental Analysis Updates, *Monthly Weather Review*, **124**(6), 1256-1271.

Bosilovich, M. G., and coauthors, 2015: MERRA-2: Initial evaluation of the climate**.** ***NASA/TM–2015–104606***, Vol. **43**, 139 pp.

Chang, Y., S. Schubert, R. Koster, A. Molod and H. Wang, 2019: Tendency Bias Correction in Coupled and Uncoupled Global Climate Models with a focus on impacts over North America. *J. Climate,* **32**, 639–661. https://doi.org/10.1175/JCLI-D-18-0598.1

Copernicus Climate Change Service (C3S), 2017: ERA5: Fifth generation of ECMWF atmospheric reanalyses of the global climate. Copernicus Climate Change Service Climate Data Store (CDS), https://cds.climate.copernicus.eu/cdsapp#!/home

Cullather, R. I., S. M. J. Nowicki, B. Zhao, and M. J. Suárez, 2014: Evaluation of the surface representation of the Greenland Ice Sheet in a general circulation model. *J. Climate*, **27**, 4835–4856, doi:https://doi.org/10.1175/JCLI-D-13-00635.1.

Danforth, C.M., E. Kalnay, and T. Miyoshi, 2007: Estimating and Correcting Global Weather Model Error. *Mon. Wea. Rev.,* **135**, 281–299, https://doi.org/10.1175/MWR3289.1.

Fan, Y., and H. van den Dool, 2008: A global monthly land surface air temperature analysis for 1948–present, *J. Geophys. Res*., **113**, D01103, doi:10.1029/2007JD008470.

Gelaro, R., and Coauthors, 2017: The Modern-Era Retrospective Analysis for Research and Applications, Version 2 (MERRA-2). *J. Climate***, 30**, 5419–5454, https://doi.org/10.1175/JCLI-D-16-0758.1.

Koster, R. D., M. J. Suarez, A. Ducharne, M. Stieglitz, and P. Kumar, 2000: A catchment-based approach to modeling land surface processes in a general model: 1. Model structure. *J. Geophys. Res*., **105**(D20), 24809-24822, doi:10.1029/2000JD900327.

Leith, C. E., 1978: Objective methods for weather prediction. *Annu. Rev. Fluid Mech*., **10**, 107–128.

Molod, A. M., L. Takacs, M. Suarez, and J. Bacmeister, 2015: Development of the GEOS-5 atmospheric general circulation model: evolution from MERRA to MERRA2. *Geosci. Model Dev.*, **8**, 1339-1356, doi:10.5194/gmd-8-1339-2015.

Moorthi, S., and M. J. Suarez, 1992: Relaxed Arakawa-Schubert: A parameterization of moist convection for general circulation models. *Mon. Wea. Rev*., **120**, 978-1002.

Putman, W., and S.-J. Lin, 2007: Finite-volume transport on various cubed-sphere grids. *J. Comput. Phys.*, **227**, 55–78, https://doi.org/10.1016/j.jcp.2007.07.022.

Reichle, R. H., and Q. Liu, 2014: Observation-Corrected Precipitation Estimates in GEOS-5. *NASA Tech. Memo. TM–2014-104606*, Vol. **35**, 18 pp., https://ntrs.nasa.gov/archive/nasa/casi.ntrs.nasa.gov/20150000725.pdf.

Reichle, R. H., Liu, Q., Koster, R. D., Draper, C. S., Mahanama, S. P., & Partyka, G. S., 2017: Land surface precipitation in MERRA-2. *J. Climate*, **30**, 1643-1664. doi: 10.1175/JCLI-D-16-0570.1.

Rienecker, M. M., and coauthors, 2008: The GEOS-5 data assimilation system-documentation of version 5.0.1 and 5.1.0, and 5.2.0. NASA Tech. Rep. Series on Global Modeling and Data Assimilation, NASA/TM-2008-104606, **27**, 92pp.

Rienecker, M.M., and Coauthors, 2011: MERRA - NASA's Modern-Era Retrospective Analysis for Research and Applications. *J. Climate*, **24**, 3624-3648. doi: 10.1175/JCLI-D-11-00015.1.

Schubert, S.D., Y. Chang, H. Wang, R. D. Koster and A. M. Molod, 2019: A Systematic Approach to Assessing the Sources and Global Impacts of Errors in Climate Models." *J. Climate*, **32**, 8301-8321, https://doi.org/10.1175/JCLI-D-19-0189.1

Takacs, L.L., M.J. Suárez, and R. Todling, 2018: The Stability of Incremental Analysis Update. *Mon. Wea. Rev.*, **146**, 3259–3275, https://doi.org/10.1175/MWR-D-18-0117.1

Wallace, J. M., and D. S. Gutzler, 1981: Teleconnections in the geopotential height field during the Northern Hemisphere Winter. *Mon. Wea. Rev.*, **109**, 784-812.

Xue, H.-L., Shen, X.-S., and Chou, J.-F., 2013: A forecast error correction method in numerical weather prediction by using the recent multiple-time evolution data. Advances in Atmospheric Sciences, 30(5), 1249–1259. https://doi.org/10.1007/s00376-013-2274-1.

Previous Volumes in This Series

Volume 1 September 1994	*Documentation of the Goddard Earth Observing System (GEOS) general circulation model - Version 1* L.L. Takacs, A. Molod, and T. Wang
Volume 2 October 1994	*Direct solution of the implicit formulation of fourth order horizontal diffusion for gridpoint models on the sphere* Y. Li, S. Moorthi, and J.R. Bates
Volume 3 December 1994	*An efficient thermal infrared radiation parameterization for use in general circulation models* M.-D. Chou and M.J. Suarez
Volume 4 January 1995	*Documentation of the Goddard Earth Observing System (GEOS) Data Assimilation System - Version 1* James Pfaendtner, Stephen Bloom, David Lamich, Michael Seablom, Meta Sienkiewicz, James Stobie, and Arlindo da Silva
Volume 5 April 1995	*Documentation of the Aries-GEOS dynamical core: Version 2* Max J. Suarez and Lawrence L. Takacs
Volume 6 April 1995	*A Multiyear Assimilation with the GEOS-1 System: Overview and Results* Siegfried Schubert, Chung-Kyu Park, Chung-Yu Wu, Wayne Higgins, Yelena Kondratyeva, Andrea Molod, Lawrence Takacs, Michael Seablom, and Richard Rood
Volume 7 September 1995	*Proceedings of the Workshop on the GEOS-1 Five-Year Assimilation* Siegfried D. Schubert and Richard B. Rood
Volume 8 March 1996	*Documentation of the Tangent Linear Model and Its Adjoint of the Adiabatic Version of the NASA GEOS-1 C-Grid GCM: Version 5.2* Weiyu Yang and I. Michael Navon
Volume 9 March 1996	*Energy and Water Balance Calculations in the Mosaic LSM* Randal D. Koster and Max J. Suarez

Volume 10 April 1996	*Dynamical Aspects of Climate Simulations Using the GEOS General Circulation Model* Lawrence L. Takacs and Max J. Suarez
Volume 11 May 1997	*Documentation of the Tangent Linear and Adjoint Models of the Relaxed Arakawa-Schubert Moisture Parameterization Package of the NASA GEOS-1 GCM (Version 5.2)* Weiyu Yang, I. Michael Navon, and Ricardo Todling
Volume 12 August 1997	*Comparison of Satellite Global Rainfall Algorithms* Alfred T.C. Chang and Long S. Chiu
Volume 13 December 1997	*Interannual Variability and Potential Predictability in Reanalysis Products* Wie Ming and Siegfried D. Schubert
Volume 14 August 1998	*A Comparison of GEOS Assimilated Data with FIFE Observations* Michael G. Bosilovich and Siegfried D. Schubert
Volume 15 June 1999	*A Solar Radiation Parameterization for Atmospheric Studies* Ming-Dah Chou and Max J. Suarez
Volume 16 November 1999	*Filtering Techniques on a Stretched Grid General Circulation Model* Lawrence Takacs, William Sawyer, Max J. Suarez, and Michael S. Fox-Rabinowitz
Volume 17 July 2000	*Atlas of Seasonal Means Simulated by the NSIPP-1 Atmospheric GCM* Julio T. Bacmeister, Philip J. Pegion, Siegfried D. Schubert, and Max J. Suarez
Volume 18 December 2000	*An Assessment of the Predictability of Northern Winter Seasonal Means with the NSIPP1 AGCM* Philip J. Pegion, Siegfried D. Schubert, and Max J. Suarez
Volume 19 July 2001	*A Thermal Infrared Radiation Parameterization for Atmospheric Studies* Ming-Dah Chou, Max J. Suarez, Xin-Zhong Liang, and Michael M.-H. Yan

Volume 20 August 2001	*The Climate of the FVCCM-3 Model* Yehui Chang, Siegfried D. Schubert, Shian-Jiann Lin, Sharon Nebuda, and Bo-Wen Shen
Volume 21 September 2001	*Design and Implementation of a Parallel Multivariate Ensemble Kalman Filter for the Poseidon Ocean General Circulation Model* Christian L. Keppenne and Michele M. Rienecker
Volume 22 August 2002	*A Coupled Ocean-Atmosphere Radiative Model for Global Ocean Biogeochemical Models* Watson W. Gregg
Volume 23 November 2002	*Prospects for Improved Forecasts of Weather and Short-term Climate Variability on Subseasonal (2-Week to 2-Month) Time Scales* Siegfried D. Schubert, Randall Dole, Huang van den Dool, Max J. Suarez, and Duane Waliser
Volume 24 July 2003	*Temperature Data Assimilation with Salinity Corrections: Validation for the NSIPP Ocean Data Assimilation System in the Tropical Pacific Ocean, 1993–1998* Alberto Troccoli, Michele M. Rienecker, Christian L. Keppenne, and Gregory C. Johnson
Volume 25 December 2003	*Modeling, Simulation, and Forecasting of Subseasonal Variability* Duane Waliser, Siegfried D. Schubert, Arun Kumar, Klaus Weickmann, and Randall Dole
Volume 26 April 2005	*Documentation and Validation of the Goddard Earth Observing System (GEOS) Data Assimilation System – Version 4* Senior Authors: S. Bloom, A. da Silva and D. Dee Contributing Authors: M. Bosilovich, J-D. Chern, S. Pawson, S. Schubert, M. Sienkiewicz, I. Stajner, W-W. Tan, and M-L. Wu
Volume 27 December 2008	*The GEOS-5 Data Assimilation System - Documentation of Versions 5.0.1, 5.1.0, and 5.2.0.* M.M. Rienecker, M.J. Suarez, R. Todling, J. Bacmeister, L. Takacs, H.-C. Liu, W. Gu, M. Sienkiewicz, R.D. Koster, R. Gelaro, I. Stajner, and J.E. Nielsen

Volume 28 April 2012	*The GEOS-5 Atmospheric General Circulation Model: Mean Climate and Development from MERRA to Fortuna* Andrea Molod, Lawrence Takacs, Max Suarez, Julio Bacmeister, In-Sun Song, and Andrew Eichmann
Volume 29 June 2012	*Atmospheric Reanalyses – Recent Progress and Prospects for the Future.* *A Report from a Technical Workshop, April 2010* Michele M. Rienecker, Dick Dee, Jack Woollen, Gilbert P. Compo, Kazutoshi Onogi, Ron Gelaro, Michael G. Bosilovich, Arlindo da Silva, Steven Pawson, Siegfried Schubert, Max Suarez, Dale Barker, Hirotaka Kamahori, Robert Kistler, and Suranjana Saha
Volume 30 December 2012	*The GEOS-iODAS: Description and Evaluation* Guillaume Vernieres, Michele M. Rienecker, Robin Kovach and Christian L. Keppenne
Volume 31 March 2013	*Global Surface Ocean Carbon Estimates in a Model Forced by MERRA* Watson W. Gregg, Nancy W. Casey and Cécile S. Rousseaux
Volume 32 March 2014	*Estimates of AOD Trends (2002-2012) over the World's Major Cities based on the MERRA Aerosol Reanalysis* Simon Provencal, Pavel Kishcha, Emily Elhacham, Arlindo M. da Silva, and Pinhas Alpert
Volume 33 August 2014	*The Effects of Chlorophyll Assimilation on Carbon Fluxes in a Global Biogeochemical Model* Cécile S. Rousseaux and Watson W. Gregg
Volume 34 September 2014	*Background Error Covariance Estimation using Information from a Single Model Trajectory with Application to Ocean Data Assimilation into the GEOS-5 Coupled Model* Christian L. Keppenne, Michele M. Rienecker, Robin M. Kovach, and Guillaume Vernieres
Volume 35 December 2014	*Observation-Corrected Precipitation Estimates in GEOS-5* Rolf H. Reichle and Qing Liu

Volume 36
March 2015

Evaluation of the 7-km GEOS-5 Nature Run

Ronald Gelaro, William M. Putman, Steven Pawson, Clara Draper, Andrea Molod, Peter M. Norris, Lesley Ott, Nikki Prive, Oreste Reale, Deepthi Achuthavarier, Michael Bosilovich, Virginie Buchard, Winston Chao, Lawrence Coy, Richard Cullather, Arlindo da Silva, Anton Darmenov, Ronald M. Errico, Marangelly Fuentes, Min-Jeong Kim, Randal Koster, Will McCarty, Jyothi Nattala, Gary Partyka, Siegfried Schubert, Guillaume Vernieres, Yuri Vikhliaev, and Krzysztof Wargan

Volume 37
March 2015

Maintaining Atmospheric Mass and Water Balance within Reanalysis

Lawrence L. Takacs, Max Suarez, and Ricardo Todling

Volume 38
September 2015

The Quick Fire Emissions Dataset (QFED) – Documentation of versions 2.1, 2.2 and 2.4

Anton S. Darmenov and Arlindo da Silva

Volume 39
September 2015

Land Boundary Conditions for the Goddard Earth Observing System Model Version 5 (GEOS-5) Climate Modeling System - Recent Updates and Data File Descriptions

Sarith Mahanama, Randal Koster, Gregory Walker, Lawrence Takacs, Rolf Reichle, Gabrielle De Lannoy, Qing Liu, Bin Zhao, and Max Suarez

Volume 40
October 2015

Soil Moisture Active Passive (SMAP) Project Assessment Report for the Beta-Release L4_SM Data Product

Rolf H. Reichle, Gabrielle J. M. De Lannoy, Qing Liu, Andreas Colliander, Austin Conaty, Thomas Jackson, John Kimball, and Randal D. Koster

Volume 41
October 2015

GDIS Workshop Report

Siegfried Schubert, Will Pozzi, Kingtse Mo, Eric Wood, Kerstin Stahl, Mike Hayes, Juergen Vogt, Sonia Seneviratne, Ron Stewart, Roger Pulwarty, and Robert Stefanski

Volume 42
November 2015

Soil Moisture Active Passive (SMAP) Project Calibration and Validation for the L4_C Beta-Release Data Product

John Kimball, Lucas Jones, Joseph Glassy, E. Natasha Stavros, Nima Madani, Rolf Reichle, Thomas Jackson, and Andreas Colliander

Volume 43
September 2015

MERRA-2: Initial Evaluation of the Climate

Michael G. Bosilovich, Santha Akella, Lawrence Coy, Richard Cullather, Clara Draper, Ronald Gelaro, Robin Kovach, Qing Liu, Andrea Molod,

Peter Norris, Krzysztof Wargan, Winston Chao, Rolf Reichle, Lawrence Takacs, Yury Vikhliaev, Steve Bloom, Allison Collow, Stacey Firth, Gordon Labow, Gary Partyka, Steven Pawson, Oreste Reale, Siegfried Schubert, and Max Suarez

Volume 44
February 2016

Estimation of the Ocean Skin Temperature using the NASA GEOS Atmospheric Data Assimilation System

Santha Akella, Ricardo Todling, Max Suarez

Volume 45
October 2016

The MERRA-2 Aerosol Assimilation

C. A. Randles, A. M. da Silva, V. Buchard, A. Darmenov, P. R. Colarco, V. Aquila, H. Bian, E. P. Nowottnick, X. Pan, A. Smirnov, H. Yu, and R. Govindaraju

Volume 46
October 2016

The MERRA-2 Input Observations: Summary and Assessment

Will McCarty, Lawrence Coy, Ronald Gelaro, Albert Huang, Dagmar Merkova, Edmond B. Smith, Meta Sienkiewicz, and Krzysztof Wargan

Volume 47
May 2017

An Evaluation of Teleconnections Over the United States in an Ensemble of AMIP Simulations with the MERRA-2 Configuration of the GEOS Atmospheric Model.

Allison B. Marquardt Collow, Sarith P. Mahanama, Michael G. Bosilovich, Randal D. Koster, and Siegfried D. Schubert

Volume 48
July 2017

Description of the GMAO OSSE for Weather Analysis Software Package: Version 3

Ronald M. Errico, Nikki C. Prive, David Carvalho, Meta Sienkiewicz, Amal El Akkraoui, Jing Guo, Ricardo Todling, Will McCarty, William M. Putman, Arlindo da Silva, Ronald Gelaro, and Isaac Moradi

Volume 49
March 2018

Preliminary Evaluation of Influence of Aerosols on the Simulation of Brightness Temperature in the NASA Goddard Earth Observing System Atmospheric Data Assimilation System

Jong Kim, Santha Akella, Will McCarty, Ricardo Todling, and Arlindo M. da Silva

Volume 50
March 2018

The GMAO Hybrid Ensemble-Variational Atmospheric Data Assimilation System: Version 2.0

Ricardo Todling and Amal El Akkraoui

Volume 51 July 2018	*The Atmosphere-Ocean Interface Layer of the NASA Goddard Earth Observing System Model and Data Assimilation System* Santha Akella and Max Suarez
Volume 52 July 2018	*Soil Moisture Active Passive (SMAP) Project Assessment Report for Version 4 of the L4_SM Data Product* Rolf H. Reichle, Qing Liu, Randal D. Koster, Joe Ardizzone, Andreas Colliander, Wade Crow, Gabrielle J. M. De Lannoy, and John Kimball
Volume 53 October 2019	*Ensemble Generation Strategies Employed in the GMAO GEOS-S2S Forecast System* Siegfried Schubert, Anna Borovikov, Young-Kwon Lim, and Andrea Molod
Volume 54 August 2020	*Position Estimation of Atmospheric Motion Vectors for Observation System Simulation Experiments* David Carvalho and Will McCarty
Volume 55 February 2021	*A Phenomenon-Based Decomposition of Model-Based Estimates of Boreal Winter ENSO Variability* Siegfried Schubert, Young-Kwon Lim, Andrea Molod, and Allison Collow
Volume 56 June 2021	*Validation Assessment for the Soil Moisture Active Passive (SMAP) Level 4 Carbon (L4_C) Data Product Version 5* John S. Kimball, K. Arthur Endsley, Tobias Kundig, Joseph Glassy, Rolf H. Reichle, and Joseph V. Ardizzone